Properties of point defects on single crystalline MgO(100) films

Anastasia Gonchar

2008

Contents

Chapter 1

Introduction

The understanding of surface properties are crucial for a variety of technological applications such as semiconductor device manufacturing, fuel cells development and catalysis. Among those heterogeneous catalysis[1] has been and still is a central technology in chemical industry [1]. The agriculture of the world has been supplied with fertilizers rich in nitrogen due to the Haber-Bosch process, where the nitrogen of the air is converted to ammonia using an iron-based catalyst. Even though this process was developed in the beginning of the 20th century, it was modern surface science which provided a microscopic understanding about 50 years later. The broader public became aware of heterogeneous catalysis more recently by the fact that catalysts are installed in every gasoline car engine to convert carbon monoxide and nitric oxides present in the exhaust to carbon dioxide and nitrogen. Nowadays, heterogeneous catalysts also play a central role in the production of most chemicals and in emerging fields such as energy storage and conversion and has applications in environmental chemistry.

In spite of the importance of heterogeneous catalysts, today's understanding of many catalytic processes at the microscopic level is often still poor. However, significant progress has been made in the last decades towards a better understanding and surface science has proven to be key in this respect. This is certainly highlighted by the 2007 Nobel Price in chemistry awarded to Gerhard Ertl for his contribution to the understanding of surface chemistry. The current limitations which render an understanding of a "real" catalyst

[1] A catalyst is defined as a substance that increases the rate of chemical reaction while being regenerated at the end of the catalytic cycle. A heterogeneous catalyst, in particular, is a substance -typically a solid- which is in a different phase than the reactants.

difficult may be subdivided into two main aspects:

i) Technical catalyst often consist of multi-component mixtures of materials such as oxides or combined oxide-metal systems. The complexity of the real systems precludes a thorough investigation of the physical and chemical phenomena that take place on the surface of commercial catalysts during a reaction. In order to overcome this problem, model catalysts with well-defined chemical and morphological properties were developed which can be studied with modern surface science techniques. This approach was very successful in gaining microscopic insight into heterogeneous catalysis, giving rise to the hope that someday entire processes may be understood [2]. Nevertheless, these systems cannot perfectly mimic the complexity of the real catalyst surfaces. This discrepancy is generally known as the *materials gap* between surface science and real catalysis.

ii) Industrial reactions proceed under conditions, e.g. high pressures, which preclude the in-situ application of typical particle based surface science techniques, leading to the so called *pressure gap*. However, strong efforts have been made to overcome this limitation. The development of various photon based techniques such as sum frequency generation or the development of a "high pressure" photoelectron spectroscopy [3] may be mentioned as examples here. Scientifically the direct transfer of surface processes observed under ideal UHV conditions to the situation at elevated pressures may be difficult, e.g. due to the presence of different surface species stable only at elevated pressure.

The investigation of heterogeneous model catalysts started out in the 1970s using metal single crystals as the simplest model for a supported metal catalyst [4]. These single crystal studies have demonstrated the relevance and utility of using simple single crystal surfaces to mimic more complex catalytic systems [5]. They also have highlighted the need for more complex model systems to address the nuances of the actual working catalysts that are not accurately depicted with single crystals [6]. To this end model systems exhibiting metal clusters supported on single crystalline oxides were developed [7], [8], [9], [10].

Among the strategies to prepare well defined, planar oxide surfaces is the cleavage of oxide single crystals or, alternatively, the growth of ultrathin oxide films on metallic supports. From an experimental point of view, the latter approach circumvents the drawback of low electrical and thermal conductivity (complicating the application of electron spectroscopies, STM and other experimental methods) of often used bulk oxides such as Al_2O_3, SiO_2 or MgO. The oxide film thicknesses range from a monolayer (ML) to a few

tens ML (<100 Å) and it was shown that even ultrathin oxide films can serve as adequate models to simulate bulk-terminated surfaces [11] although it is important to check for this validity in each case separately.

MgO is an ideal system [12] for experimental studies in surface science since (a) it is highly ionic, (b) it has a simple rock-salt-type crystal structure (Fig. 1.1), which renders it relatively easy to characterize, and (c) it can be prepared as a thin film on different substrates. Stoichiometry, structure and morphology have been investigated for MgO films grown on Ag(001) e.g. [17], [49], [16], Fe(001) [20], [22] and Mo(001) [36], [48]. In addition, Mo(100) surfaces are used as supports, which offer the possibility to treat the films at high temperatures, but exhibit the larger lattice mismatch with the MgO as compared to Ag(100) (5.5 % vs. 2.9 %) [36]. High temperature deposition or post-growth annealing, which is not applicable for Ag substrates, is usually performed to improve the film morphology and reduce its defectiveness. Initial studies on thin MgO films on Mo(001) studies [36] by the means of LEED, Auger electron spectroscopy (AES), temperature programmed desorption (TPD) and high-resolution electron energy-loss spectroscopy (HREELS) have shown that in spite of a 5.5% lattice mismatch between MgO(100) and Mo(100), an ordered MgO film can be formed on the substrate with its (100) face parallel to the (100) face of Mo (Fig. 1.2), where the MgO[001] direction is actually rotated by 45° with respect with that of Mo[001]. More recently a combined LEED and STM investigation [19] has shown that there is a coincidence pattern with the Mo support in the low coverage regime, a dislocation network at medium thickness which relaxes with increasing film thickness to give a rather flat and defect-poor MgO surface for thicker layers. This is in line with CO adsorption and LEED experiments which concluded in films with extended terraces and only a small amount of defects for films of typically 10-30 ML thickness [18], [47].

Very often the chemical and physical properties of solid materials are not controlled by the ideal terraces, but by structural defects (Fig. 1.3). Apart from extended defects such as steps or dislocation lines, point defects such as impurity atoms or ion vacancies are an important class of defects. On oxide surfaces oxygen vacancies are a prominent example of the latter class [21]. These sites can be created by thermal and chemical treatments, or irradiation with particles [37]. Historically, these centers were often called

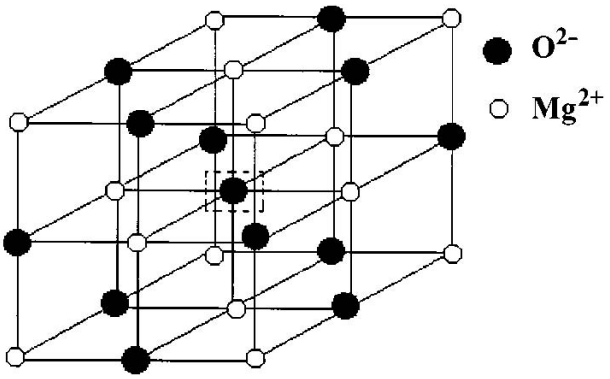

Figure 1.1: Magnesium oxide structure

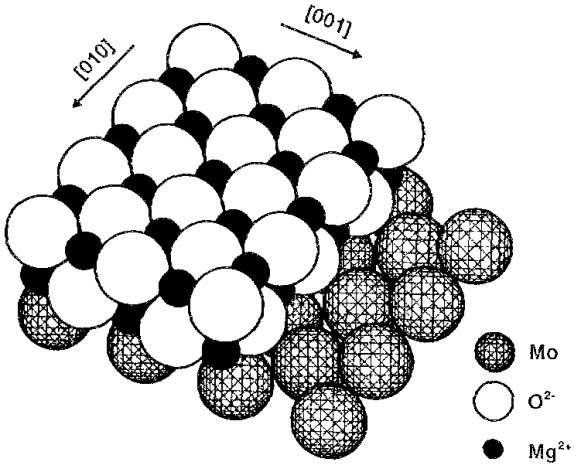

Figure 1.2: Magnesium oxide (100) on molybdenum (100) substrate. Adopted from [36].

color centers or F-centers[2] (from Farbe, the German word for color) due to the fact that their presence add color to a crystal. The effect is due to the formation of defect states in the band gap of the wide band gap insulators which can be excited by visible or near UV light. Thus, it become clear that defects play an important role for the optical, electronic and transport properties of the material as well as the chemistry of its surface. A detailed understanding of point defects and their control at the atomistic level is therefore important to understand the chemistry and physics of oxide surfaces. On oxides F-centers can exist in three electronic states, depending on the charge present in the vacancy [39]. Diamagnetic oxygen vacancies can be either neutral, F^0, or doubly charged F^{2+}, with two or no electrons trapped in the cavity, respectively. The removal of an O^- ion results in F^+ with one electron, trapped in the cavity. F^+ centers can be observed and characterized by electron paramagnetic resonance (EPR) spectroscopy. In case of a simple cubic lattice of a highly ionic oxide the charge state is sufficient to describe isolated anion vacancies in the bulk. On the surface the situation is more complex, because the surface analogous -usually designated with the subscript s- may exist not only on perfect terrace sites but also at structural defects present on every surface such as steps, corners, or kinks. Energetically the latter are strongly preferred as compared to the ideal terrace sites and calculation suggest that diffusion from the terrace to low coordinated sites has to be expected [23]. Chemically, F_s centers on oxide surfaces are expected to be able to donate or abstract electrons to adsorbed molecules or deposited metal clusters [26], [40], which is considered an important mechanism to change the catalytic properties of metal deposits or adsorbates. Even though the importance of surfaces containing F_s centers is generally accepted, experimental characterizations of these centers and a subsequent analysis of their influence on adsorbed species is rather scarce. Only recently it was shown that Au clusters nucleated at to color centers on MgO(100) films become indeed negatively charged [76]. To get a deeper insight into the mechanism of the interaction of metal aggregates with such defects a systematic studies with different metals are required. Hereto, this thesis reports on an experimental study of copper deposited on a single crystalline MgO(100) previously used for the characterization of Au particles to highlight similarities and differences for the two systems.

[2]It should be noted here that nowadays the term F center should be used to designate anion vacancies which is not consistently found in the literature.

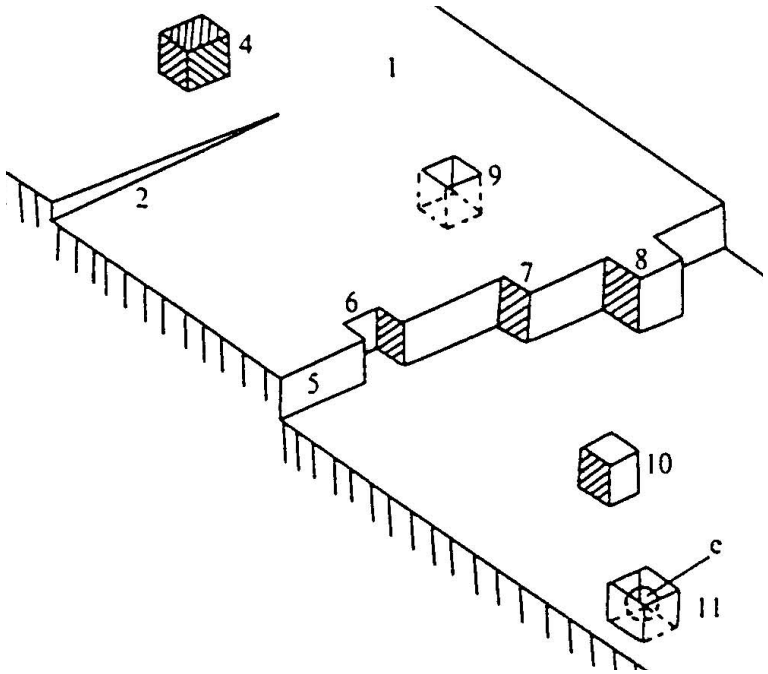

Figure 1.3: Simple defects, which are often found in a low-index crystal face. 1. A perfect flat face itself — a terrace; 2. a screw dislocation; 4. an impurity adatom; 5. a monatomic step at the surface — an edge; 6. a vacancy in the edge; 7. a step in the edge — a kink; 8. an adatom situated upon the edge; 9. a vacancy in the terrace; 10. an adatom at the terrace; 11. the vacancy at the terrace, where electron is trapped.

Chapter 2

Review of techniques

2.1 Electron Paramagnetic Resonance Spectroscopy

Electron paramagnetic resonance (EPR), also known as electron spin resonance (ESR), is a powerful technique for examining the environment of unpaired electrons. EPR is the process of resonant absorption of radiation by unpaired electrons in the presence of a strong magnetic field.

Electrons possess a property called spin. The corresponding magnetic moment is proportional and collinear with the spin vector. Along a quantization axis, the spin vector of the electron can take the value $\pm\frac{1}{2}$. In the presence of an external magnetic field the degeneracy of the two spin states is lifted by the so-called Zeeman effect and the electron's magnetic moment orients itself either parallel or antiparallel to the field. The energies corresponding to the two allowed orientations of the spin are expressed as:

$$E = g\mu_B BS,$$

where g is electronic g-value, B — the field strength of the external magnetic field, μ_B — the Bohr magneton, S the spin projection on the field.

The energy difference (Fig. 2.1) between these two Zeeman levels ($\Delta m_s = \pm 1$ is:

$$\Delta E = g\mu_B B.$$

According to the Planck's law, electromagnetic radiation will be absorbed if:

$$\Delta E = h\nu,$$

where ν is the frequency of the radiation, h is Planck's constant.

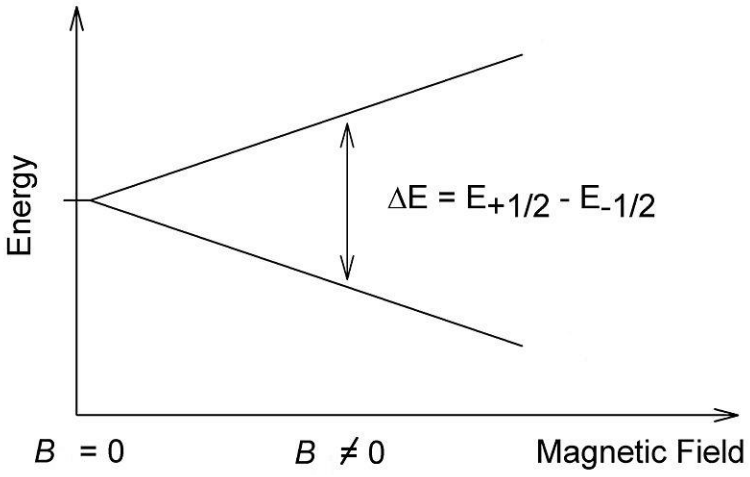

Figure 2.1: Zeeman splitting

The spin magnetic moment may be influenced by various interactions with the electron environment when the unpaired electron is located in a molecule or compound. These interactions result in a shift of the EPR line with respect to the position of the free electron. The spin Hamiltonian $\mathcal{H}$ used to describe typical interactions that may be present can be written as follows:

$$\mathcal{H} = \mathcal{H}_{\mathrm{eZ}} + \mathcal{H}_{\mathrm{nZ}} + \mathcal{H}_{\mathrm{hfs}} + \mathcal{H}_{\mathrm{zf}} + \mathcal{H}_{\mathrm{Q}}.$$

where eZ denotes the electronic Zeeman, nZ the nuclear Zeeman, hfs hyperfine interaction, zf the zero field splitting, and Q quadrupole interactions. In case of the F-centers discussed in this thesis this hamiltonian can be simplified to a single term, namely the electronic Zeeman interaction, because all other terms can be neglected for the understanding these systems. Thus, in the following the discussion is focused the electronic Zeeman interaction which is most generally written as follows:

$$\mathcal{H}_{\mathrm{eZ}} = \mu_B \, \mathbf{B}^{\mathrm{T}} \, \tilde{g} \, \mathcal{S} = \mu_B \begin{bmatrix} B_x & B_y & B_z \end{bmatrix} \begin{bmatrix} g_{xx} & g_{xy} & g_{xz} \\ g_{yx} & g_{yy} & g_{yz} \\ g_{zx} & g_{zy} & g_{zz} \end{bmatrix} \begin{bmatrix} \mathcal{S}_x \\ \mathcal{S}_y \\ \mathcal{S}_z \end{bmatrix}.$$

$\tilde{g}$ is a symmetric tensor, which can be always diagonalized:

$$\tilde{g} = \begin{bmatrix} g_x & 0 & 0 \\ 0 & g_y & 0 \\ 0 & 0 & g_z \end{bmatrix}.$$

The important consequence of this anisotropic interaction is that the resonance position measured for a particular center depends on the orientation of the center with respect to

the static magnetic field. The precise values of the g-tensor depend on the electronic structure of the atom or molecule as well as it environment under consideration. Conversely the measured g-tensor components as well as it orientation with respect to environment can be used to gain information about the system. This aspect has become more important in recent years due to the development of powerful theoretical methods to calculate these parameters for realistic models [25].

In practice, EPR samples consist of a large ensemble of paramagnetic species populating the different spin states according to thermodynamic equilibrium. For a two state system this may be given by the Maxwell-Boltzmann equation:

$$\frac{n_{\text{upper}}}{n_{\text{lower}}} = exp\left(\frac{-\Delta E}{kT}\right),$$

where n_{upper} is the number of paramagnetic centers occupying the high energy state, k is the Boltzmann constant and T is the temperature in Kelvin. In a typical cw-EPR experiment the incident microwave power is chosen such that this population difference is not significantly altered. Which means that relaxation rate has to be high as compared to the absorption probability to avoid saturation effects. For paramagnetic systems this population difference is rather small. As a consequence the temperature dependence of the signal intensity can be described by Curie's law:

$$M = C\,\frac{B}{T},$$

where M is the magnetization (amount of magnetic moment per unit volume), C is a material-specific Curie constant and T is the temperature. Thus, the signal intensity increases as the inverse of the temperature with decreasing temperature.

For typical magnetic fields in the range of 1 Tesla, the required radiation belongs to microwave region. The most commonly used EPR spectrometer operate between 9-10 GHz (X-band) which correspond to a field around 0.35 T for the free electron g-value.

A typical cw-EPR system consists of (Fig. 2.2) :

i) a microwave source, supplying monochromatic radiation whose power is controlled by attenuator between the source and the sample.

ii) a waveguide system to propagate the microwave radiation from the source to the resonant cavity.

iii) a resonator with a high Q-factor (Fig. 2.3), to take advantage of the enhanced electromagnetic fields in the resonator structure for the excitation of magnetic dipole

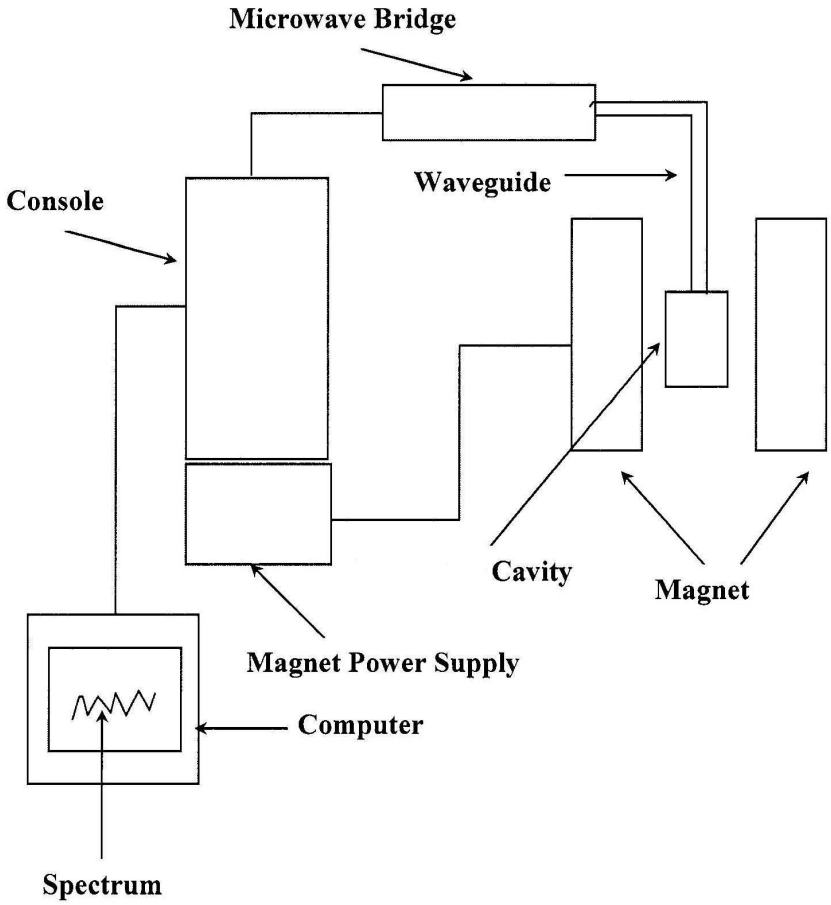

Figure 2.2: Schematics of an EPR experiment

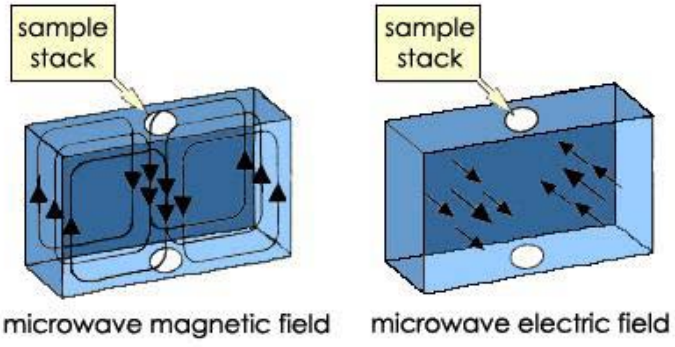

Figure 2.3: Field distribution in a TE_{102} EPR cavity used in our experiments

transitions.

iv) a magnet system capable of providing a homogeneous field over the sample volume.

v) detection, modulation and recording systems.

Due to the use of a resonator cw-EPR spectrometer operate at a fixed frequency and vary the "static" magnetic field to fulfill the resonance condition. However, the absorbed microwave power is very weak which renders a direct detection of this absorption difficult. In order to improve on this the static magnetic field is modulated periodically (typically at 100 kHz) and the signal is detected using a phase sensitive detection scheme also known as a Lock-In technique. As a result, the detected signal appears as a first derivative of the adsorption spectrum with respect to the magnetic field. For comparative purposes the resonance field is not well suited as it depends on the the precise frequency of the microwave radiation used. Instead the spectra are analyzed in terms of the characteristic magnetic parameters; e.g. in case of a system governed purely by Zeeman interaction by the g-matrix (see above).

2.2 Infrared spectroscopy

Infrared spectroscopy (IR) is the subset of photon based spectroscopies that deals with electric dipole excitations in the infrared region of the electromagnetic spectrum. Infrared radiation has wavenumbers from roughly 13000 to 10 cm^{-1}, or wavelengths from 0.78 to 1000 μm.

As a molecule is absorbed on a surface, it exhibits a variety of vibrations, both internal as well as external ones. These vibrations may be associated with a distortion of the electrical charge distribution of the system and can be resolved into dipole, quadrupole, octopole contributions. These vibrations can couple to the electric field vector of incident IR radiation if the corresponding vibration is associated with a change of the dynamic dipole moment of the system.

Infrared spectroscopy was among the first techniques to be applied to the direct characterization of adsorbates [33]. The early studies employed transmission infrared spectroscopy, in which the infrared beam passes through a suitably prepared sample [34], [35]. Such a setup is not suitable for the investigations of non transparent metal substrates which require the use reflectance spectroscopy. An evaluation of the Frensel equations proves IR reflection absorption spectroscopy (IRAS) to be done best in grazing incidence geometry. The reflection at conductive surface has the important additional consequence that the s-polarized field component is quenched by the image dipole present in the metal surface (Fig. 2.4). In turn, IRAS on metal surfaces is only capable to excite vibrations with a component of dynamic dipole moment aligned perpendicular to surface, a phenomenon also known as the metal-surface selection rule.

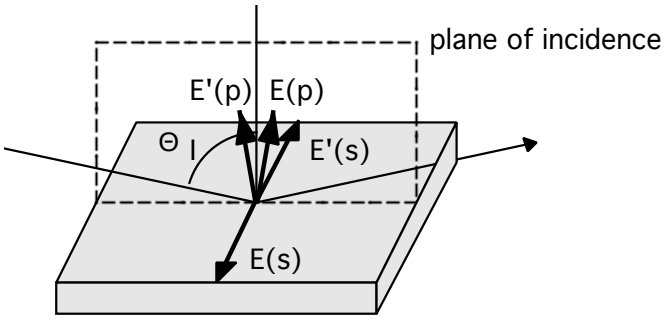

Figure 2.4: Electric vectors of the s- and p-polarized components of radiation incident on a metal surface. Primed and unprimed vectors refer to reflected and incident rays, respectively.

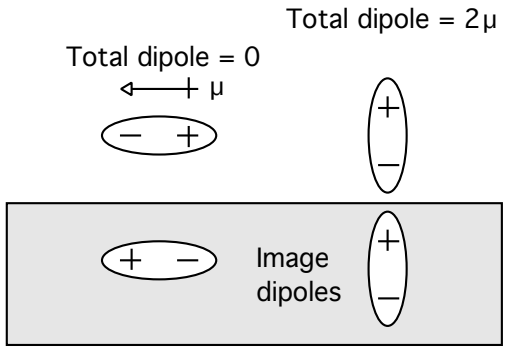

Figure 2.5: Surface dipole selection rule

Technically the IR spectra are measures using a Fourier transform spectrometer. The main component of such a spectrometer is a Michelson interferometer (Fig. 2.6) which consists of a moving mirror, a fixed mirror, and a beamsplitter positioned at an angle of 45 degrees with respect to these mirrors. Radiation from the broadband IR source is collimated and directed into the interferometer, and impinges on the beamsplitter. At the beamsplitter, divides the IR beam into two portions. One half is transmitted to the fixed mirror and the remaining half is reflected to the moving mirror. After the divided beams are reflected from the two mirrors, they are recombined at the beamsplitter. The resulting beam then passes through or is reflected at the sample and is focused on the detector. The detector signal is recorded as an interference pattern of the measured signal intensity with respect to the position of the movable mirror (determined by a HeNe-laser). From this interference pattern the entire spectrum can be generated by a simple Fourier-transformation.

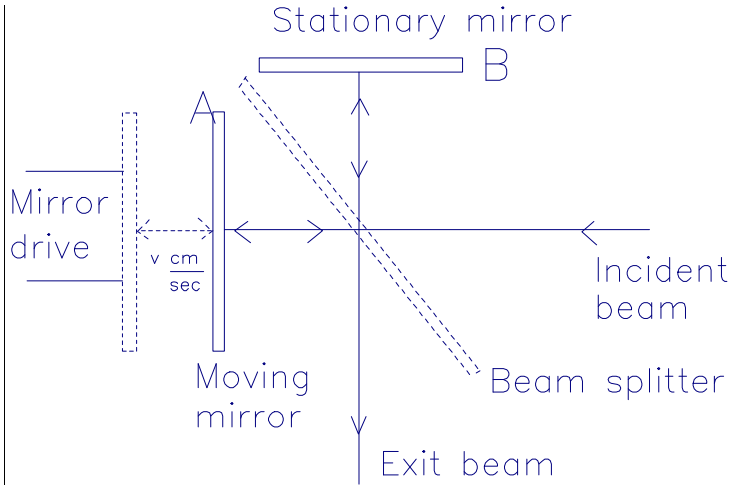

Figure 2.6: Schematics of a Michelson interferometer

However, a simple analysis of a spectrum taken from a surface is hampered by the small absorption of the surface species as compared to the spectral response of the spectrometer. In order to improve the signal to background ratio of the spectroscopy an IR spectrum is typically measured in a two steps. As a first step a spectrum of the surface without the species under consideration is measured as a background spectrum. This spectrum accounts for the combined performance of source, interferometer, and detector as well as contributions spurious oscillators in the optical path. In a second step the oscillator of interest e.g. the probe molecule is absorbed on the surface and a spectrum is collected. It contains absorption bands from the sample and the background. The final spectrum is created by division of the latter by the background spectrum.

2.3 Thermal Programmed Desorption

Temperature Programmed Desorption (TPD) also known as Thermal Desorption Spectroscopy (TDS) is a technique to study adsorbates on surfaces. The experiment utilizes temperature-programming to discriminate between processes with different activation parameters.

A typical experiment (Fig. 2.7) consists of the following steps:

i) Preparation of a clean surface.

ii) Adsorption the species of interest.

iii) Increasing the temperature of the sample in linear fashion and monitor the desorbing species by a mass spectrometer. Typical heating rates are between 0.5 K/s and 10 K/s.

With increasing temperature adsorbed species will desorb from the surface according to their binding energy. Concomitantly the partial pressure of this species will first rise until the species characterized by the corresponding binding energy are desorbed and the partial pressure drop down at higher temperatures. This results in a peak in the pressure versus temperature plot. The temperature of the desorption peak, its shape as well as its dependence on the initial surface coverage and heating rate can be analyzed to provide information about binding energies and other quantities such as lateral interactions between the adsorbate.

The following points are worth noting :

i) The area underneath a peak is proportional to the amount of adsorbate characterized a particular adsorption enthalpy, i.e. proportional to the surface coverage of this species.

ii) The kinetics of desorption (obtained from the peak profile and the coverage dependence of the desorption characteristics) give information on the state of aggregation of the adsorbed species e.g. molecular v's dissociative.

iii) The position of the peak (the peak temperature) is related to the enthalpy of adsorption, which is in simple cases directly related to the binding energy to the surface.

Even though TPD can provide a wealth of information concerning the state of adsorbates on surfaces it is important to remember that a thorough analysis requires a whole set of experiments taken for different surface coverage and heating rates.

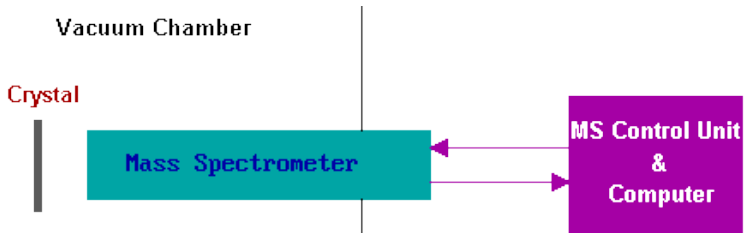

Figure 2.7: Schematics of a TPD experiment

2.4 Low Energy Electron Diffraction

Low-energy electron diffraction (LEED) is a technique used to characterize periodic structures of surfaces. In the experiment a beam of low energy electrons (typically in the range 20-600 eV, which corresponds to wavelengths in the order of the atomic distances in crystals) is directed onto a sample in order to observe diffraction spots characteristic for the periodic structure of the sample surface. The surface sensitivity of LEED follows from the short mean free path (a few Åat 100 eV) of the elastically scattered electrons which give rise to the characteristic diffraction spots.

LEED may be used in one of two ways:

i) Qualitative: the diffraction pattern is recorded and analysis of the spot positions yields information on the size and symmetry of the unit cell.

ii) Quantitative: there are two flavors depending on the information of interest: I/V or tensor LEED: the intensities of the various diffracted beams are recorded as a function of the incident electron beam energy. Together with appropriate modeling this data allows a quantitative determination of atomic position within the periodic structure. Spot Profile Analysis (SPA) LEED is a variant of the above mentioned experiment as it monitors the profile of LEED spots as a function of the energy. This allows to extract information on periodic structures with larger real space periodicity e.g. mosaicity.

Within this thesis LEED will only be used as a qualitative tool to verify the long range order of oxide films.

A LEED instrument usually consists of an electron gun and detector System in a backscattering geometry (Fig. 2.8). Monochromatic electrons are emitted by a cathode filament which is at a negative potential, typically 10-600 V, with respect to the sample. They are accelerated and focused into a beam, typically about 0.1 to 0.5 mm wide, by a series of electrodes that serve as electron lenses. Some of the electrons incident on the sample surface are backscattered elastically, and in case the surface has long range order diffraction occurs. This typically requires a single crystal region surface as large as the electron beam. The LEED detector is a retarding field analyser containing three or four hemispherical, concentric grids and a phosphor screen. The potentials of the grids are chosen such that only the elastically-scattered electrons can penetrate and contribute to the diffraction pattern while the lower energy (secondary) electrons are repelled by the grids of the energy filter.

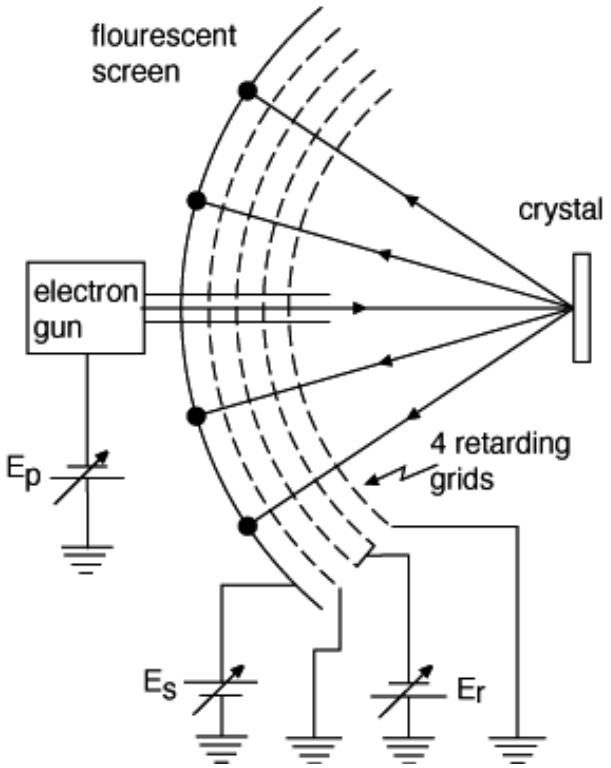

Figure 2.8: Schematics of a LEED experiment

Chapter 3

Experimental Details

3.1 Experimental Setup

Studies of clean surfaces demand Ultra High Vacuum (UHV) in the range of 10^{-8} Pascal (10^{-10} mbar). UHV requires the use of special materials in creating the vacuum system and extreme cleanliness to maintain the vacuum system. The mean free path of a gas molecule at 10^{-9} mbar is approximately 40 km, so gas molecules will collide with the chamber walls many times before colliding with each other. Thus, almost all interactions take place on various surfaces in the chamber.

The experiments have been performed in an ultrahigh vacuum apparatus [41] with the base pressure of 2×10^{-10} mbar shown schematically in Fig. 3.1. The chamber is pumped with a stack of an ion-getter, a turbo-molecular and a titanium sublimation pump.

The apparatus combines a preparation stage located in the upper chamber, which is equipped with a LEED/Auger system, a mass spectrometer for TPD experiments and residual gas analysis as well as evaporation sources and a quartz microbalance for the preparation of the sample. In addition the apparatus allows for an infrared spectroscopic characterization using grazing incidence reflection absorption IR (IRAS) (middle part) and EPR spectroscopic investigations at the bottom of the chamber.

The long travel manipulator allows a manipulation of the sample inside the chamber in X, Y, and Z direction as well as a rotation around the long axis. The sample is mounted at the end of a helium cryostat which is mounted inside the manipulator and allows cooling of the sample down to 30 K.

The sample itself consists of a cut and polished Mo(100) single crystal serving as the

substrate for the MgO(100) film preparation. The crystal is mounted on tungsten rods and held by a 0.3 mm molybdenum wire loop sitting in slits on three sites of the crystal (Fig. 3.2). The tungsten rods are connected to a sapphire block which is attached to the primary heat exchanger of the helium cryostat. Due to the electrical isolation of the sample, the sample can be heated directly by passing current trough the molybdenum loop or by electron impact. A W/Re (5% and 26% Re) thermocouple spot welded to the top edge of the crystal is used to measure the temperature of the substrate. The sample could be heated up to 1100 K via direct heating and up to 2300 K using an electron beam from an external filament.

TPD measurements have been performed by placing the sample less than 1 mm away from the cup around the quadrupole mass spectrometer. The sample was resistively heated with a heating rate of 0.5 K/s as measured by a commercial controller (Schlichting Elektronische Instrumente).

With the manipulator, the sample can be transferred to an intermediate position to perform Infrared Reflection Absorption Spectroscopy (IRAS) measurements. A BIO-RAD type FTS-40 VM FTIR spectrometer extended by a home made optics to allow for grazing incident reflection measurements was used. The spectrometer is evacuated by a rotary pump to avoid gas phase absorption by CO_2 and water. During the measurement, dried nitrogen flows through the spectrometer serving as a gas cushion for the movable mirror of the Michelson interferometer. The coupling of the spectrometer to the vacuum chamber is realized via two Viton sealed KBr windows which allow for measurements in the low 10^{-10} mbar range. The reflected infrared radiation is measured by a mercury–cadmium–telluride (MCT) detector, which is liquid nitrogen cooled. For the IRAS experiments CO was used as a probe molecule and the sample was exposed at 35 K to different CO amounts up to saturation coverage. The IRAS spectra were recorded with 4 cm^{-1} resolution. For each spectrum one thousand scans were accumulated and recorded at 35 K if not stated otherwise. Background spectra were recorded using the same settings.

For the IR and TPD measurements high purity CO was passed through a liquid nitrogen trap for further purification prior to its introduction into the vacuum chamber.

From the IR intermediate position the sample may be moved into the EPR stage after passing a metal-glass connection. This ends in a quartz tube which sits in the bore of an EPR cavity (type TE_{102} from Bruker). The cavity is part of a Bruker EMX

spectrometer equipped with a high-current 12" Varian electromagnet to create the static magnetic field. The magnet can be moved in and out of the measurement position on rails to allow adjustment of sample and cavity. For EPR measurements radiation in the X-band ranging between 9-10 GHz is used. The incident microwave power used in the experiments was chosen to avoid saturation effects. The EPR spectra were recorded with a modulation amplitude of 4 G. Typically EPR spectra were taken at 35 K and 100 scans were accumulated to obtain a reasonable signal to noise ratio.

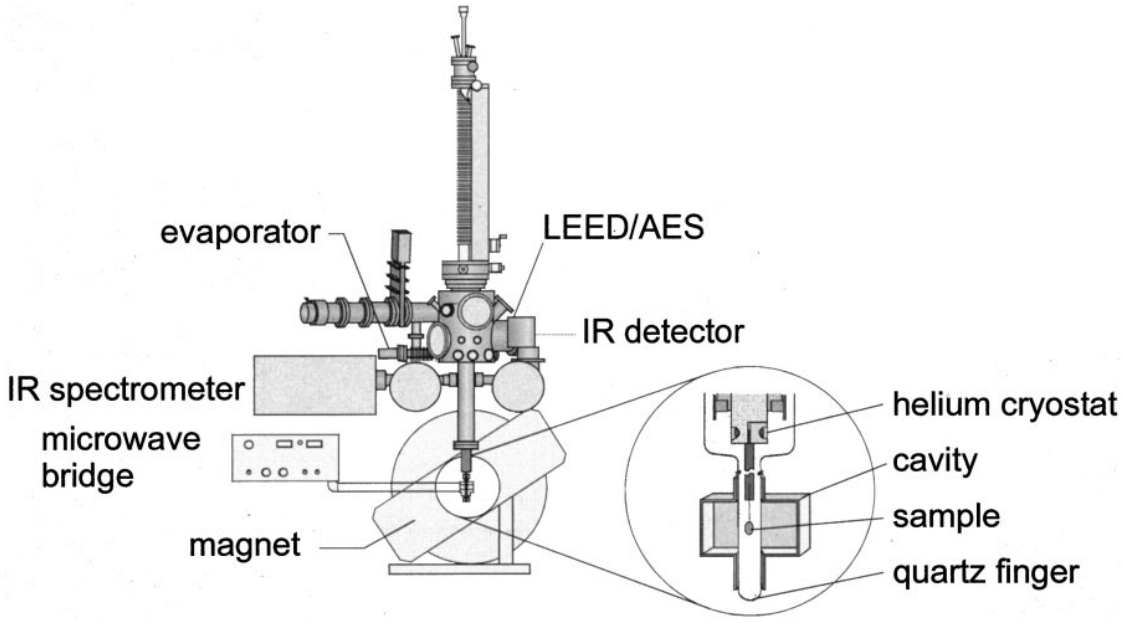

Figure 3.1: Schematics of the experimental setup

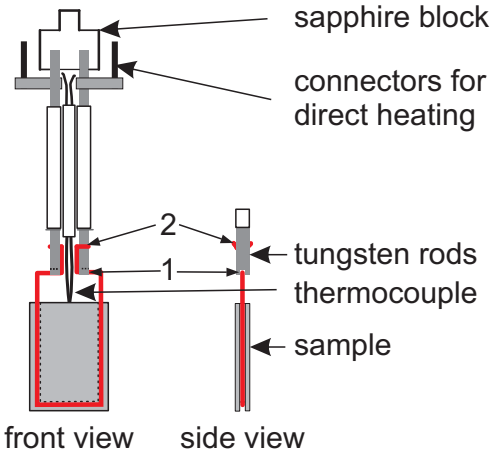

Figure 3.2: Sample

3.2 Sample preparation

The Mo substrate was cleaned by oxidation with O_2 at 1500 K and a pressure of 1×10^{-6} mbar followed by subsequent flashes to 2300 K in UHV. The MgO(100) films have been prepared by evaporation of Mg in a background pressure of oxygen (1×10^{-6} mbar) onto the clean Mo(100) substrate held at 600 K [36]. The Mg was evaporated from a carbon crucible using a commercial electron beam evaporator (Omicron EFM3). The sample was biased to the voltage of the evaporant during metal deposition to avoid acceleration of metal ions onto the surface. The deposition rate was 1 monolayer (ML) MgO/min. The thickness of the film was controlled by quartz microbalance.

The long range order as judged by LEED can be improved by annealing the MgO film up to 1100 K for about 10 min. Throughout this paper we will refer to the well ordered film as an "annealed" film, while preparations lacking this annealing step are called "rough" MgO films.

For the investigation of paramagnetic species on single crystal surfaces, absolute sensitivity is of paramount importance. It has been shown previously that EPR spectroscopy has the necessary sensitivity to detect paramagnetic species in submonolayer coverage under UHV conditions [43]. The pristine MgO film exhibits no EPR signal above the noise floor of the apparatus; therefore the number of singly charged color centers was estimated to be lower than 1×10^{12} on this surface [48].

To create surface color centers [42], the MgO film was bombarded with electrons of 100 eV energy at room temperature extracted from a filament. The time of exposure and emission current at fixed energy were chosen to get a nominal electron dosage of 1200 electrons per surface oxygen ion (e^-/O_2).

If not stated otherwise, Cu atoms were deposited at 35 K on a 20 ML thick MgO(100) film grown on a Mo(100) substrate. The Cu atoms were evaporated using a commercial electron beam evaporator (Omicron EFM3) at a deposition rate of 1 Å Cu per 20 min. The sample was biased to the voltage of the evaporant during Cu deposition. The deposited amount was calibrated by a quartz microbalance and is reported as the nominal thickness of a hypothetical continuous layer of the metal deposited on the MgO film given in Å. Throughout this paper we will refer to the nominal thickness, as for instance the term 1 Å Cu, is an abbreviation for copper deposits prepared by deposition of 1 Å of copper and is not intended to characterize the actual size of possible Cu clusters.

Chapter 4

Results and Discussion

4.1 Interaction of CO with MgO(100) film

In this chapter we will discuss the interaction of CO[1] with regular, low-coordinated sites as well as F_s^+ and F_s centers of single crystalline MgO(100) film. We will start with well ordered annealed films, exhibiting large terraces, then will turn to rough films with increased amount of corners and edges and, finally, will discuss the binding of CO on F_s^+ and F_s centers.

The crystallinity of 20 ML thick MgO(100) films on Mo(100) was verified using LEED. The LEED pattern of a well ordered, annealed film is shown in Fig. 4.1. The quality of the annealed MgO(100) film is proved by its characteristic (1×1) LEED pattern exhibiting sharp diffraction spots. The rough film has the same diffraction pattern, but broader diffraction spots.

First, we will revisit infrared spectra of CO adsorbed on the surface of MgO(100). The interaction of CO with the MgO surface was studied theoretically [57], [58], [10], [46] and experimentally for powder, single crystals and thin films e.g. [45], [47], [44], [18], [61]. The binding mode of CO on the regular MgO surface and the influence of differently coordinated binding sites on the CO infrared frequency shift was investigated theoretically [46]. It is now established that that CO binds with the carbon end down to surface magnesium sites and the binding is almost purely due to electrostatic interactions. A blue shift of the

[1] The reasons for the use of carbon monoxide include those which make it a favorite molecule of surface science in general, chiefly its ease of handling and the sensitivity of the molecule's vibrational frequency to the manner in which it is bonded to the substrate.

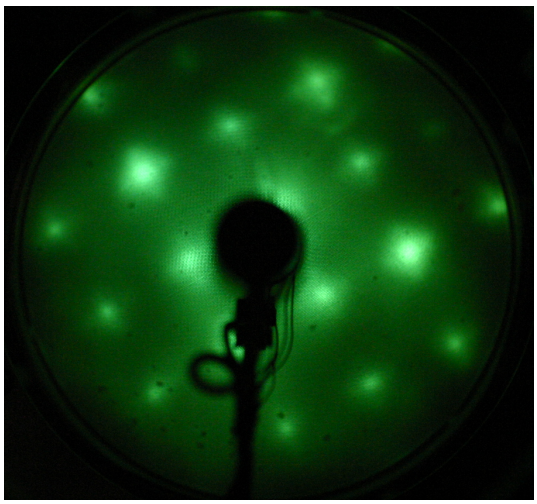

Figure 4.1: LEED pattern of a thin, single crystalline, annealed 20 ML thick MgO(100) film

CO stretching mode with respect to the stretching mode of gaseous CO (2143.3 cm^{-1}) has been explained being due to the repulsive interaction between the carbon atom and the surface anions. A reduction of the coordination number of Mg sites, e.g. at steps or corners, leads to a stronger binding. Concomitantly, a shift of the CO stretching frequency to higher energies is observed, which arises from a stronger polarization of the adsorbed molecule at these sites.

The p-polarized infrared spectra taken after saturating the surface of a vacuum-cleaved MgO single crystal CO below 40 K with CO exhibit three bands at 2151, 2137 and 2132 cm^{-1} [44]. Excitation with s-polarized light reveals a spectrum with a single line at 2132 cm^{-1}. In combination with temperature dependent measurements, LEED, and helium atom scattering experiments the main band at 2151 cm^{-1} was assigned to perpendicular oriented CO molecules adsorbed on regular terrace sites, while the latter two bands were attributed to the in-phase and out-of-phase vibrational excitation of tilted CO in a c(4×2) overlayer, respectively. The signal at 2132 cm^{-1} was assigned to the out-of-phase vibrational excitation of the tilted CO dipole, which corresponds to a parallel orientation of the dynamic dipole moment with respect to the surface. The characteristic c(4×2) superstructure as well as the two bands for the in-phase and out-of-phase vibrational excitation disappear at temperatures above 40 K.

The infrared spectra taken after saturating the surface of a well ordered 20 ML MgO(001) thin film supported on Mo(001) at 30 K with CO is characterized by a relatively sharp

band at 2152 cm^{-1} with a shoulder on the high frequency wing and a pronounced feature at 2138 cm^{-1} [47]. The lack of the band at 2132 cm^{-1} is due to the metal surface selection rule which limits the observable transitions to those with dynamic dipole moments oriented perpendicular to the surface. TPD experiments on well annealed thin MgO(001) films show a CO desorption behavior which is very similar to that of single crystals, namely, the main desorption peak corresponding to CO desorption from terrace sites is found at 52 K, followed by a broad and less intense desorption feature up to 100 K which is assigned to CO bound to low coordinated Mg ions [18][47].

Our IR spectra on the well ordered annealed MgO film are shown in Fig. 4.2. In the low coverage regime, a CO band at 2170 cm^{-1} is observed with a shoulder at 2180 cm^{-1}. At monolayer coverage the spectrum is characterized by a relatively sharp band at 2153 cm^{-1} with a shoulder on the high frequency wing. The main IR band at 2153 cm^{-1} is associated with CO adsorbed on five-coordinated Mg ions. The pronounced shoulder at the high energy side of the band at 2153 cm^{-1} has been assigned to CO adsorbed on step or edge sites of the MgO islands. The red-shift of the infrared band with increasing coverage is understood as being due to lateral repulsion of CO molecules, which leads to weaker binding to the surface and a reduced Pauli-repulsion of the CO molecules and the oxide.

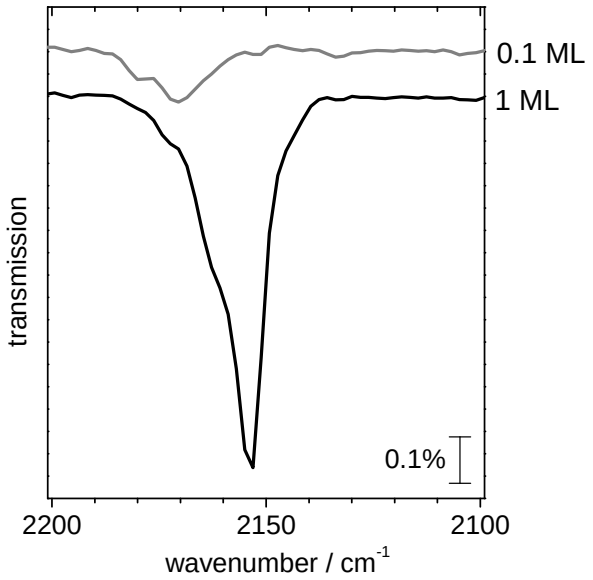

Figure 4.2: CO IR spectra of a well ordered annealed MgO(100) film

TPD experiments (Fig. 4.3) performed here show a main desorption peak corresponding to CO desorption from terrace sites at 65 ± 5 K, followed by a broad and less intense desorption feature up to 100 K which is assigned to CO bound to edges and corners. This

shift of the TPD peak as well as the absence of the IR band at 2138 cm^{-1} is explained by a reduction of the CO coverage which is due to a surface temperature of about 50 K which is in perfect agreement with IR and TPD studies reported in the literature [18],[47].

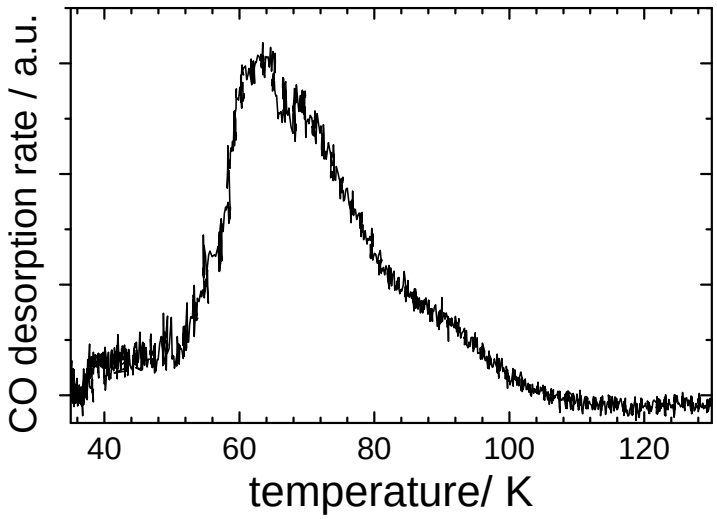

Figure 4.3: TPD spectrum of an annealed MgO(100) film

The influence of concentration of low-coordinated Mg sites on infrared spectra can be seen in Fig. 4.4, where the spectra after CO adsorption on rough MgO(001) film are presented. At saturation CO coverage the spectrum is characterized by a sharp band at 2164 cm^{-1} with a shoulder on the low frequency wing. The increased defectiveness from annealed to rough film is seen from the larger intensity ratio between the signal corresponding to defect sites and regular terrace sites. However, a quantification of the ratio between terrace and defect sites based on the infrared intensities is not straightforward. The complication arises from the fact that an intensity borrowing from the low frequency to the high frequency peak can occur for strongly dipolar coupled systems [62], [56].

Finally, we present experiments of CO adsorbed on electron bombarded MgO(100) films which exhibit surface color centers. Beside the paramagnetic F_s^+ centers the surface exhibits diamagnetic F_s^0 centers. These sites were characterized by combining angular dependent EPR measurements and low temperature STM and STS experiments which shows them to be located predominantly at the edges and corners of the MgO islands [48], [49]. Therefore, rough films, which contain an increased number of low-coordinated sites, allow to increase the number of color centers.

After electron bombardment an almost symmetric EPR signal a resonance line around $g \approx 2.000$ was observed for the magnetic field oriented in the surface plane as shown in

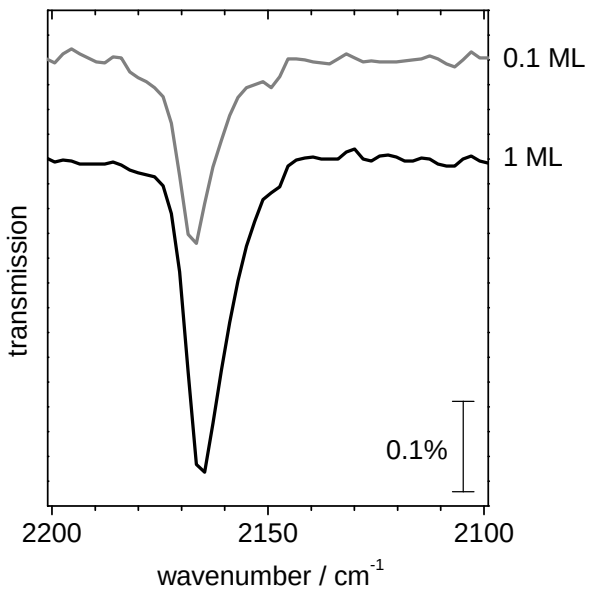

Figure 4.4: CO IR spectra of a rough MgO(100) film

the upper trace of Fig. 4.5. The surface nature of the obtained color centers was proven by their reaction with molecules from the gas phase. Dosing 1 ML equivalent O_2 at 35 K to the electron bombarded MgO film results in disappearance of the characteristic F_s^+ centers signal which is replaced by a complicated structure with $g \approx 2.004$, $g \approx 2.010$, $g \approx 2.040$ and $g \approx 2.055$ as shown in second trace of Fig. 4.5. It is expected that these signals correspond to paramagnetic oxygen species created by the reaction of molecular oxygen with the color centers. Different oxygen radicals species, namely, several kinds of O^- (M, N, Q) [87], [86], superoxide O_2^- [89], [88] and ozonide ion O_3^- [90] have been observed experimentally on MgO powders and were studied theoretically. The known g-values are collected in Table 4.1.

The resonance at $g \approx 2.055$ points to the presence of O_2^- radicals, because a signal at such a low field is not compatible with the principal g-tensor components observed for O^- species. However, this does not allow to rule out the presence of O^- species which might be responsible for some of the signals observed at higher fields. It is worth mentioning that the signal shape suggests that the species have a rather well defined geometry with respect to the surface. This can be inferred from the signals at low fields which exhibit a broad but simple derivative shape while the signal around g = 2.010 - 2.004 might be a due to superposition of several orientations. An assignment of the signal to specific species based on this data is difficult, because the observed signal positions are most

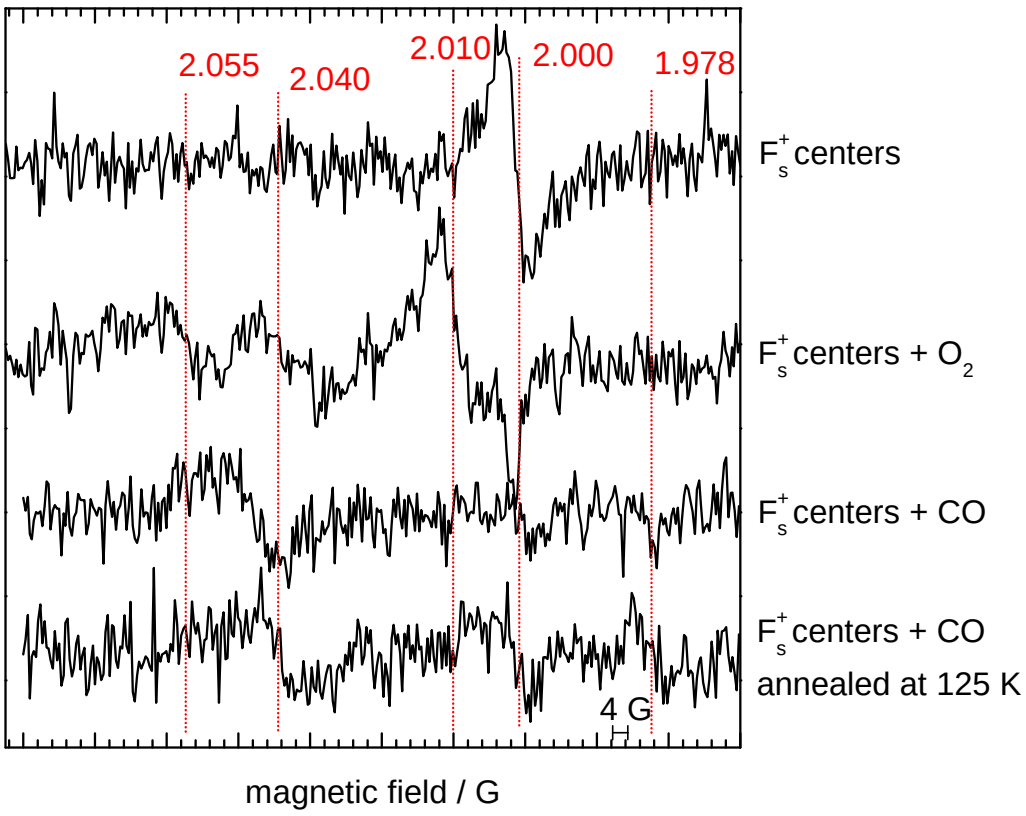

Figure 4.5: EPR spectra of an electron bombarded MgO(100) film (upper trace), of electron bombarded MgO(100) film adsorbed 1 ML O_2 (second trace), electron bombarded MgO(100) film adsorbed 1 ML CO (third trace) and electron bombarded MgO(100) film adsorbed 1 ML CO annealed at 125 K (lower trace)

Table 4.1: g-values of oxygen radicals species on MgO powders surface. Data from [87], [86], [89], [88], [90]

Species	$\mathbf{g}_x$	$\mathbf{g}_y$	$\mathbf{g}_z$
O^- (M) [87], [86]	2.002	2.002	2.046
O^- (M) [87], [86]	2.0016	2.0016	2.046
O^- (N) [87], [86]	2.002	2.002	2.036
O^- (N) [87], [86]	2.0016	2.0016	2.035
O^- (Q) [87], [86]	2.002	2.002	2.024
O^- (Q) [87], [86]	2.0016	2.0016	2.018
O_2^- [88]	2.0023	2.007	2.082
O_3^- [90]	2.0014	2.018	2.012

likely not reporting on the principal components of the g-tensor, but determined by the particular orientation of the local g-tensor framework of the different species with respect the surface. Additional experiments in particular angular dependent measurements, which are challenging for the given signal to noise ratio, are needed to allow for a more detailed interpretation of the data.

Similarly, the color center containing MgO surface could be exposed to CO molecules from the gas phase. As seen in the third trace of Fig. 4.5 exposure to saturation coverage of CO leads to an almost complete annihilation of the paramagnetic color center signal which strengthen the argument about the surface character of the paramagnetic center. As the adsorption perturbs the color center significantly it is also to be expected that the CO molecules is perturbed when adsorbed at color centers. To this end IRAS measurements have been performed in order to investigate the impact of color centers onto the adsorbed CO molecules. The first three traces shown in Fig. 4.6 present the infrared spectra of color center containing MgO films as a function of CO coverage (1/10 up to saturation coverage). Apart from the features of the rough films discussed above, two new bands related to the presence of color centers around 1850 cm^{-1} (A) and 1720 cm^{-1} (B) appear. At low CO coverage the IR spectrum shows a broad band at 1880 cm^{-1} and a peak at 1740 cm^{-1}. With increasing CO coverage the bands shift to lower frequencies, 1850 cm^{-1} and 1710 cm^{-1} at full coverage. A strong red shift of the IR signal of CO bound to color centers with respect to terrace or low coordinated sites (2152 and 2164 cm^{-1}) can

be explained by the electron donating character of the color centers leading to substantial charge transfer onto the CO molecules. The enhanced line width of the band A as compared to band B might be due to a superposition of several peaks or stronger coupling to CO molecules in the vicinity, however, a more detailed analysis is not possible at the moment.

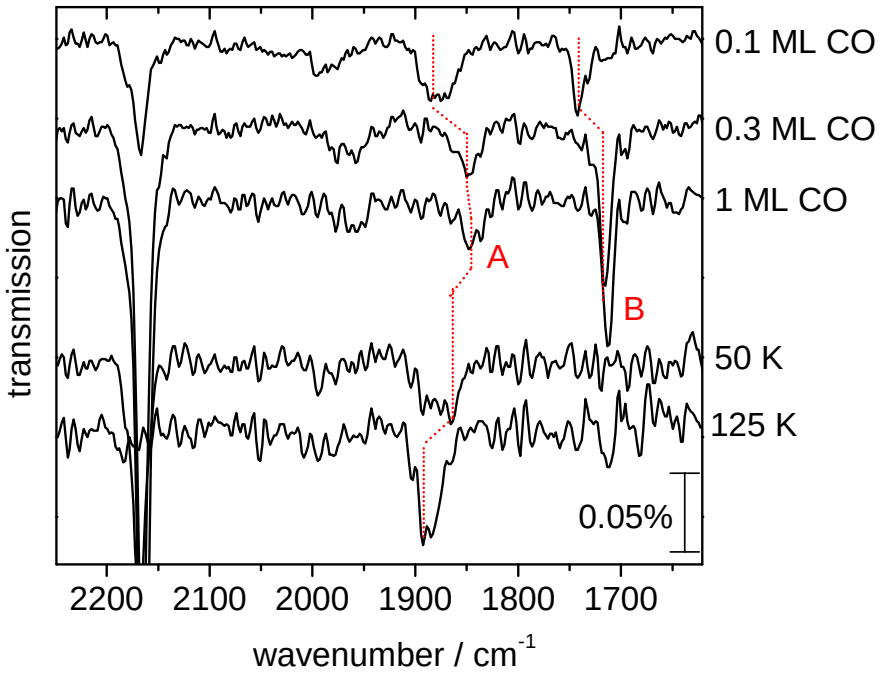

Figure 4.6: IR spectra of an electron bombarded MgO(100) film up to a CO saturation monolayer coverage and annealing experiments

The thermal stability of the bands A and B is found to be drastically different. After heating up the sample to 60 K peak B disappears. The peak can be restored by re-adsorption of CO even after annealing to 300 K. This indicates, that the disappearance of the IR signal at 60 K is due to CO desorption, but the color center underneath remains intact. In contrast to that signal A is considerably more stable. With increasing the annealing temperature, the band A gains intensity and shifts back to higher wavenumbers as shown by the IR spectra taken after annealing to 60 K and 125 K at the bottom of Fig. 4.6. The CO desorption from the sites, giving rise to this band, occurs at temperatures higher than 300 K. Thus we can conclude, that the absorbtion energy for CO at site A is much higher than for the site B. Based on the previously acquired knowledge these two IR band should correspond to CO bound to F_s^+ and F_s^0 centers, respectively. However, a direct assignment of the signals to the species is not straightforward. An experimental

study on the interaction of CO at 77 K with the diamagnetic and paramagnetic centers on MgO powder was performed by Marchese *et al* [55]. They have produced color centers by contacting the surface of MgO powder with Mg vapors. Additional IR bands in the range of 1850–1700 cm^{-1} were observed, which is in agreement with the present observations, and based on the position these signals have been tentatively assigned to CO^-. Theoretical studies on the interaction of CO molecule with oxygen vacancies on the MgO(100) surface have been performed by Ferrari and Pacchioni [54]. It was found, that CO interaction of CO (C-side down) is purely repulsive when approaching F_s^+ as well as F_s^0 centers of the MgO surface. However, at short distances from the surface, a bound state is found which corresponds to a charge transfer complex of the type CO^-/F_s^{2+} or CO^-/F_s^+. When CO interacts with a neutral F_s center, the bound state, CO^-/F_s^+, is found to be higher in energy than the neutral dissociation limit and represents only a local minimum on the potential energy surface, independent of the calculation details (CO basis set, inclusion of surface relaxation, etc.) (Fig. 4.7). When CO interacts with a paramagnetic F_s^+ center, the charge transfer state, CO^-/F_s^{2+}, is energetically close to the corresponding "neutral" dissociation limit and it was not possible to establish if the global reaction is exothermic or endothermic, because the result depends on computational treatment (Fig. 4.8). The computed CO stretching frequency on F_s^+ and F_s centers is 1864 and 1783 cm^{-1}, respectively. Comparing the observed IR spectrum with theoretical predictions it is possible to assign the signal at 1850 cm^{-1} to CO adsorbed on paramagnetic F_s^+ centers while the signal at 1710 cm^{-1} correspond to CO adsorbed diamagnetic F_s centers. This assignment needs further theoretical support, since the theoretical model considers the oxygen vacancy to be on terrace, while the color centers present on the MgO surface are located at edges and corners [48], [49]. In addition, the calculations cannot account for the large difference in stability of the charge transfer complexes observed in the experiments.

Based on the IR spectroscopy and the theoretical calculation the interaction of CO with paramagnetic color centers should result in the formation of CO^- radicals. In order to prove the existence of CO^- radicals on the electron bombarded MgO film, it is worth to come back to the EPR experiments briefly mentioned above. A closer look at the EPR spectrum taken after saturating the electron bombarded MgO film at 35 K with CO reveals not only a quenching of characteristic signal of F_s^+ centers, but also the appearance

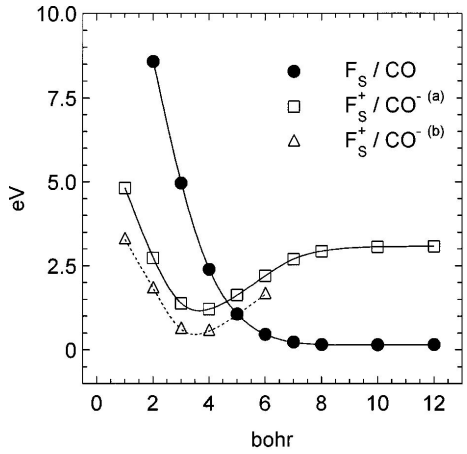

Figure 4.7: Potential energy curves for the interaction of CO with MgO oxygen vacancies: CO on a F_s center, CO^- on a F_s^+ center basis set A (a), CO^- on a F_s^+ center basis set B (b). Details are described in [54]. The picture was adopted from [54].

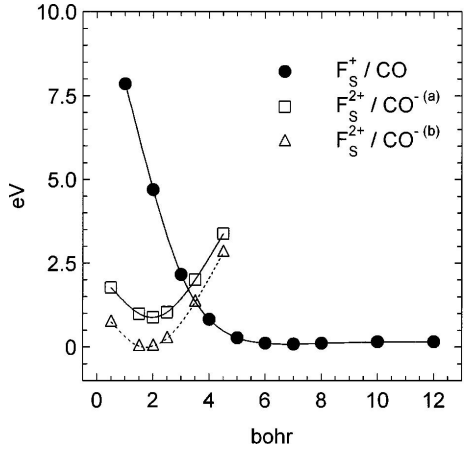

Figure 4.8: Potential energy curves for the interaction of CO with MgO oxygen vacancies: CO on a F_s^+ center, CO^- on a F_s^{2+} center basis set A (a), CO^- on a F_s^{2+} center basis set B (b). Details are described in [54]. The picture was adopted from [54].

of a signal with $g \approx 2.051$ (Fig. 4.5, third trace). The EPR signature of CO^- radicals have been described in the literature by the group of Giamello who studied the interaction of carbon monoxide with electron-rich magnesium oxide surfaces prepared by contacting the powder with vapors of metallic magnesium or alkali metal (Li or Na) [50]. The paramagnetic signal observed at 100 K after this treatment exhibits an anisotropic g tensor with $g_1 \approx 2.0041$, $g_2 \approx 2.0014$ and $g_3 \approx 1.9817$, the later component having a rather large linewidth. No paramagnetic signal with g value higher then g value of free electron was expected for CO^- radical. Thus, the large signal observed at $g \approx 2.051$ is incompatible with CO^- radicals. On the other hand the signal is rather close to the resonance lines observed for oxygen based radicals (see second trace in Fig. 4.5). An interesting observation is made after the annealing the system to 125 K. This leads to the appearance of two signals around 2.004 and 1.978, and a shift of the signal around 2.051 to $g \approx 2.040$ (Fig. 4.5, lower trace). Note, that the appearance of the EPR signals is accompanied by an increase of the IR intensity of the species around 1880 cm^{-1}.

The experimental observations might be explained as follows. After a CO adsorption on electron bombarded MgO, the EPR signal from paramagnetic centers is quenched, which proves the interaction of CO with the F_s^+ centers of the surface. The IR data confirm the adsorption of CO on color centers, because of the appearance of two new peaks A and B not observed for regular and low-coordinated MgO sites. The strong shift and drastically different thermal stability of IR peaks A and B indicate rather different absorbtion properties of CO on these sites pointing to a different nature of the underlying adsorption site, which is consistent with CO adsorption on F_s^+ and F_s^0 centers. The absence of CO^- radical signal after absorbtion of saturation CO coverage might be explained by a strong interaction of the CO^- radical with CO adsorbed in the vicinity, which can result in broadening of the signal. This is in line with the observed broadening in the IR spectra for high coverage of CO. After heating up the system to 125 K, the EPR signal previously assigned with CO^- radical [50] appears. At these temperature CO is already desorbed from terrace as well as low coordinated sites of the MgO surface, which is confirmed by IR and TPD studies, and IR peak A exhibits the shift to higher wavenumbers and an apparent increase of the intensity. Thus, we assume, that CO^- is not coupled any more with CO bound on Mg sites, therefore we are able to observe an CO^- signal with g-value around 2.004 and 1.978. The fact, that we detect g-value of 1.978, although it is broad for

powder spectra, indicates on the existence of a preferable orientation of CO^- radical at the MgO film surface. The existence of the signal with $g \approx 2.051$ after CO absorbtion and its transformation in $g \approx 2.040$ can be explained by the presence of O^- radical, since it is compatible with literature data [87], [86] and our EPR observation after O_2 absorbtion, discussed above. Wether this signal is due to the cleavage of CO molecules, which would imply the formation of carbon deposits, cannot be clarified at this point.

To summarize, in this chapter we have discussed the interaction of the CO molecule with MgO single crystalline thin films, exhibiting F_s^+ and F_s centers. Two new IR bands due to CO bound on color centers have been observed around 1850 cm^{-1} (A) and 1710 cm^{-1} (B). Based on experiments performed on MgO powders [50], [55] and theoretical predictions [54], these signals are assigned to $CO^{(\delta-)}$ species formed by an electron transfer from color centers onto the CO molecules. In addition, band A is tentatively assigned to CO^-/F_s^{2+} charge transfer complexes, created from CO bound on paramagnetic F_s^+ centers, and band B to the formation of CO^-/F_s^+ complexes from CO bound on F_s^0 centers.

4.2 Cu atoms and clusters on MgO(100) films

This chapter summarizes the experiments to characterize Cu deposits on MgO(100) surfaces. IR spectroscopy utilizing CO as a probe molecule served as the main tool which is amended by TPD and EPR spectroscopic investigations. This project was initiated to compare the interaction of Cu adsorbed on color centers with Au deposits which have been previously investigated [76]. Such a comparison requires knowledge about the properties of Cu adsorbed on regular MgO surfaces as well as other defects such as steps, corners, or kinks which will always be present. Thus, the following sections will first describe experiments on films free of color centers to establish a proper basis for the subsequent investigation of the interaction with color centers. In order to understand the interaction with defects other than color centers in more detail, experiments were done not only on well annealed films exhibiting large terraces and comparatively small number of defects but also on rough films characterized by significantly smaller island sizes, hence, larger number of line defects, corners, or kinks.

4.2.1 Cu on pristine MgO(100) films

As a first step 2 Å copper were deposited at 45 K on an annealed MgO film. The top three traces of Figure 4.9 show IR spectra after exposing different amounts of CO. on 2 Å Cu deposited at 45 K on an annealed MgO film. The spectra taken at 45 K show two characteristic features. A signal at 2160 cm^{-1} which corresponds to CO adsorbed on MgO terrace sites as discussed in detail in the previous chapter. A new peak is observed around 2100 cm^{-1} which grows with increasing CO coverage and shifts from 2095 cm^{-1} at low CO coverage to 2100 cm^{-1} at saturation coverage. At higher coverage this peak is accompanied by a broad feature at about 2050 cm^{-1}.

The lowest trace of Fig. 4.10 shows the CO-TPD spectrum taken after saturating 2 Å Cu grown at 35 K on an annealed MgO(001) film with CO. The TPD spectrum (shown is only the high temperature part were no desorption from the MgO surface is found (see Fig. 4.3)) shows a broad desorption peak starting at around 130 K, with a maximum at about 200 K and a high temperature cutoff at 250 K.

Various Cu single crystal surfaces have been extensively studied by means of IRAS and TPD. At saturation coverage Cu(111) [92] and Cu(100) [91] surfaces show a single band

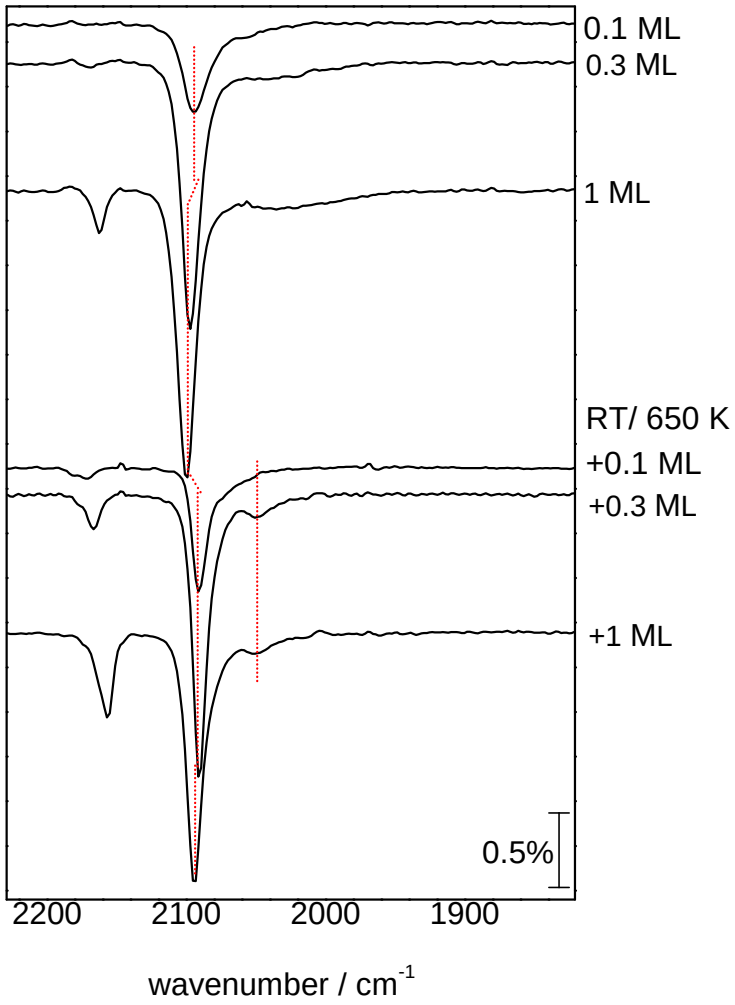

Figure 4.9: IR spectra of 2 Å Cu grown at 35 K on annealed MgO(100) film and of 2 Å Cu grown at 35 K and annealed to 650 K/grown at 300 K on annealed MgO(100) film

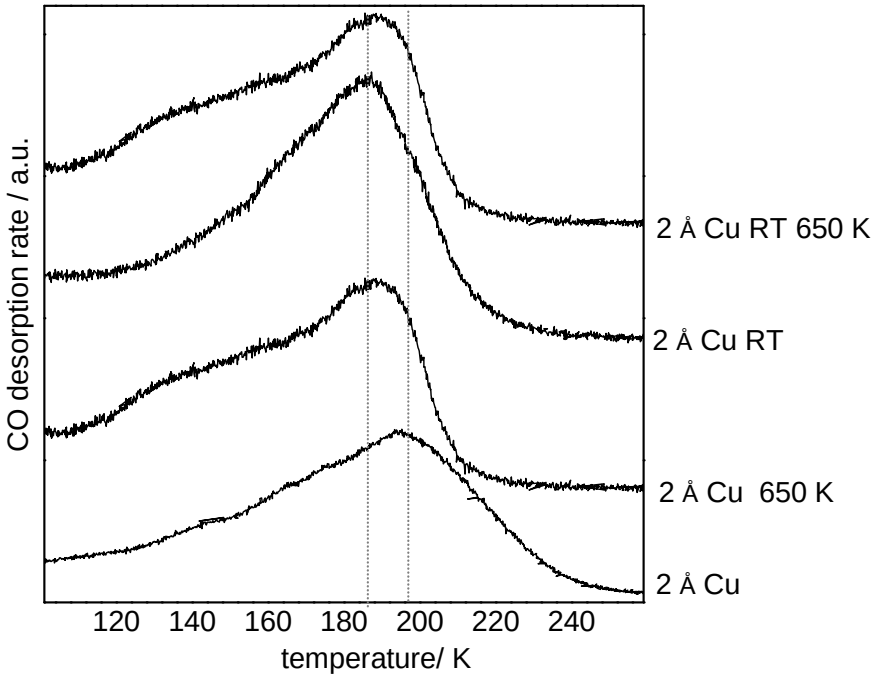

Figure 4.10: TPD spectra of 2 Å Cu on annealed MgO(100) film

around 2065 cm^{-1} and 2080 cm^{-1}, respectively. The more open (110) surface exhibits a band at slightly higher energy (2090 cm^{-1}) [63]. However, more recent studies have shown that the IR-spectra are prone to changes in the line shape due to intensity transfer. A prominent example is the case of a Cu(16,15,0) surface, where nominally 16 atoms wide (110) terraces are separated by monatomic steps, which exhibits a feature above 2100 cm^{-1} at CO saturation coverage and a second weaker band at about 2090 cm^{-1} [56]. The high energy feature corresponds to CO bound on step sites and its intensity which should nominally be about 1/16th of the terrace intensity, is strongly enhanced by intensity borrowing due to dipolar coupling. In addition, peaks in the region of 1835-1810 cm^{-1} were found for Cu(111) which has been assigned to bridged bonded CO [69], [70], [92]. The latter are not typical for copper, they have only been observed at high CO coverage and low temperatures. *Ab initio* calculations [71] of CO adsorption on several low and high Miller index surfaces of Cu show the vibrational frequencies of CO at bridge sites in 1880-1910 cm^{-1} range.

TPD studies of CO molecules adsorbed on differently oriented copper surfaces [97], [98], [99] as well as higher index surfaces which expose different amounts low coordinated sites (step, kink) [74] have been studied experimentally. In case the experiments are done at low coverage to avoid the formation of compressed superstructures CO is bound to on-top sites

and the corresponding desorption temperature range from 170 K for closed packed to 250 K for open surfaces and surfaces exposing step and kink sites. In addition, it shows that low temperature desorption peaks in the range 120-170 K observed for high CO coverage is due to lateral repulsion in the compressed CO layers and for some surfaces due to the population of bridged sites. This is in line with *ab initio* calculations [71] of CO adsorption on several low and high Miller index surfaces of Cu revealing the adsorption energy to increase as the coordination of the adsorption site decreases.

Based on the data known from experiments on single crystals the observed IR and TPD results can be interpreted in a straight forward manner. First, the presence of a large signal of CO bound to MgO sites confirms the growth of Cu particles on the MgO surface, given the fact that the deposited amount is nominally sufficient to grow a "continuous" copper film.[2] This is expected from a thermodynamic point of view [84] and in line with reports in the literature on the mode of Cu growth on MgO surfaces [64], [84], [81], [82]. For example, Zhou and Gustafsson have used medium energy ion scattering and found three dimensional islands on UHV cleaved MgO(001) single crystal surfaces [64]. Consistently, first principles density functional calculations show that Cu-Cu interactions are stronger than Cu-MgO surface interactions, and, in turn, three dimensional structures are preferred [81]. The IR signal at 2100 cm^{-1} is compatible with CO bound to open surfaces such as the (110) surface or low coordinated sites. The low growth temperature makes it rather likely that the Cu particles do not exhibit the thermodynamic equilibrium shape, but expose a rather large fraction of low coordinated sites do to kinetic limitations of the growth at low temperature. This is also consistent with the TPD results which renders desorption above 200 K to be due to open surfaces or low coordinated sites while the low temperature side would also be compatible with more densely packed surfaces. The presence of the latter can be inferred from the presence of the peak around 2050 cm^{-1}.

The sample investigated so far was grown at low temperature and the structure of the particles is expected to be strongly influenced by kinetic limitations. In order to test this scenario further the samples were annealed to 650 K which should allow the particles to relax towards the thermodynamic equilibrium, and may also give rise to Ostwald ripening of the particles (growth of the large particles at the expense of the small ones). Adsorption

[2]This can be inferred from the crystallographic data of bulk Cu which crystallizes in a face centered cubic lattice with lattice constant of 3.65 Å.

of CO on the annealed sample gives rise to an IR band at 2087 cm^{-1} with a shoulder at low frequencies for low CO coverage which shifts to 2095 cm^{-1} at saturation coverage (see Fig. 4.10). In addition, a pronounced feature at 2050 cm^{-1} is observed at saturation CO coverage. The corresponding TPD spectrum, taken after saturating the surface with CO (Fig. 4.10, second trace), exhibits a desorption peak at 185 K with a low temperature shoulder around 130 K.

Along the same line it is expected that growth of Cu at higher temperatures will also result in the formation of larger and better faceted particles. Deposition of 2 Å Cu at 300 K leads to the same IR spectra observed for the annealed system discussed above. An identical IR spectrum is also observed after annealing the 300 K deposits to 650 K. The TPD spectra show a slightly more complex picture. The spectrum taken after saturating 2 Å Cu grown at 300 K with CO (Fig. 4.10), third trace) exhibit a desorption peak at 185 K as found for the annealed low temperature deposits, but the TPD signal has an additional shoulder on the high temperature side while the low temperature shoulder at about 130 K is much less developed. In contrast to that, annealing of this system results in a TPD spectrum (Fig. 4.10, upper trace) which is virtually identical to the one of the annealed, low temperature deposit.

In combination with the knowledge from single crystal surfaces, the current data shows that annealing gives rise to the formation of Cu particles with an increased number of low index facets (Fig. 4.11) which can can be inferred from the higher IR intensity of the signal associated to CO adsorbed on terrace sites (2050 cm^{-1}). The observed infrared intensities might be obscured by intensity borrowing effects due to dipolar coupling. This kind of intensity transfer was proposed to be dominating in IR spectra of small copper particles [93]. However, the above interpretation is corroborated by the TPD results which shows the expected shift of the desorption maximum to low temperature. In addition, a low temperature desorption features develops which can be associates with the formation of high coverage CO phases on larger low index facets. In this respect please note that the particles grown at 300 K are somewhat intermediate between the low temperature deposits and the annealed system (peak at 185 K, high temperature shoulder, lack of peak at 130 K). The TPD results suggest that these particles have a larger fraction of facets than system grown at low temperature, but exhibit a larger number of defects as compared to the annealed particles. It is also worth mentioning that TPD seems

to be more sensitive to these more subtle effects than IR. The latter techniques reveals indistinguishable spectra for both the annealed and the 300 K deposits, while the TPD spectra reveals differences.

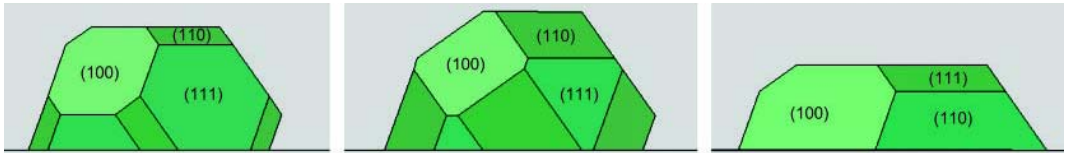

Figure 4.11: An example of Cu nanoprticles on oxide support. The picture was adopted from [83].

The introduction of additional defect sites such as F-centers might change the particles size distribution considerably towards smaller particles. In addition, it is expected that charge donation effects, which have been observed for Au particles, will be most important for small particles. Therefore, it is important to study not only rather large particles, but also to learn about the properties of small particles or even atomic species. In order to prepare smaller particles 1 Åcopper was deposited at 35 K on an annealed MgO(001) film. Fig. 4.12 shows the infrared spectra as a function of CO coverage (4 top traces) as well as annealing experiments (4 lower traces). Besides the feature corresponding to CO on MgO ($\tilde{2}060$ cm^{-1}), the IR spectra show two peaks. A signal around 2015 cm^{-1} (D) and a peak at 2080 cm^{-1} which shifts slightly to the blue (5 cm^{-1}) with increasing coverage and was previously assigned to CO bound on Cu particles. Peak D appears at a CO coverage of $\tilde{0}$.2 ML at 2018 cm^{-1} and gains intensity with increasing coverage. Concomitantly the signal shifts to lower frequency (2012 cm^{-1}) and broadens which points to a coupling of these species with surrounding CO molecules. The latter effect may also be responsible for the observed red-shift.

The relative stability of the two species was investigated by annealing experiments. With increasing annealing temperature the peak at 2085 cm^{-1} becomes broader and more asymmetric. After annealing to 130 K the maximum is shifted to 2097 cm^{-1} and the peak shows a shoulder on the low frequency side. The signal intensity, however, is not significantly changed. It should be noted that the shift to higher frequencies is unexpected based on the coverage dependence of the IR bands which always shows a blue shift with increasing coverage. In addition, this shift is correlated with the disappearance of peak D at 130 K. Prior to its reduction the latter peak shifts back to higher frequencies, but the

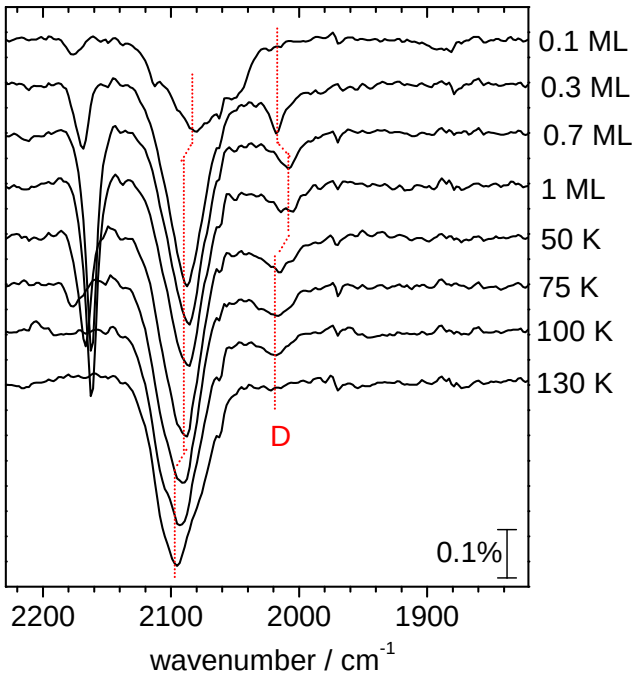

Figure 4.12: IR spectra of 1 Å Cu grown at 35 K on annealed MgO(100) film

signal remains much broader than it was after initial CO adsorption at low temperature. The shift can be explained by a decrease in dipole-dipole coupling with CO molecules on the MgO surface while the origin of the line broadening remains speculative at this point. One possible reason would be the population of different sites due to mobility of these species.

Annealing the system to 650 K and subsequent adsorption of CO up to saturation coverage results in a disappearance of the low energy peak (D). The corresponding IR spectra is characterized by the peak of CO on MgO and a relatively sharp peak at 2095 cm^{-1} with a rather small shoulder on the high frequency wing (Fig. 4.13).

Both systems were also investigated by TPD. The spectra of the pristine deposits after saturating the system with CO (Fig. 4.14, lower trace) show a rather broad desorption peak with a maximum at around 200 K which extends up to 240 K. In addition a small peak is observed at 140 K. In contrast to that the annealed system exhibits a CO-TPD spectrum (Fig. 4.14, upper trace) with a maximum around 180 K. Even though the spectrum has a long tail to low temperature a pronounced shoulder around 130 K as observed for the pristine particles is not visible.

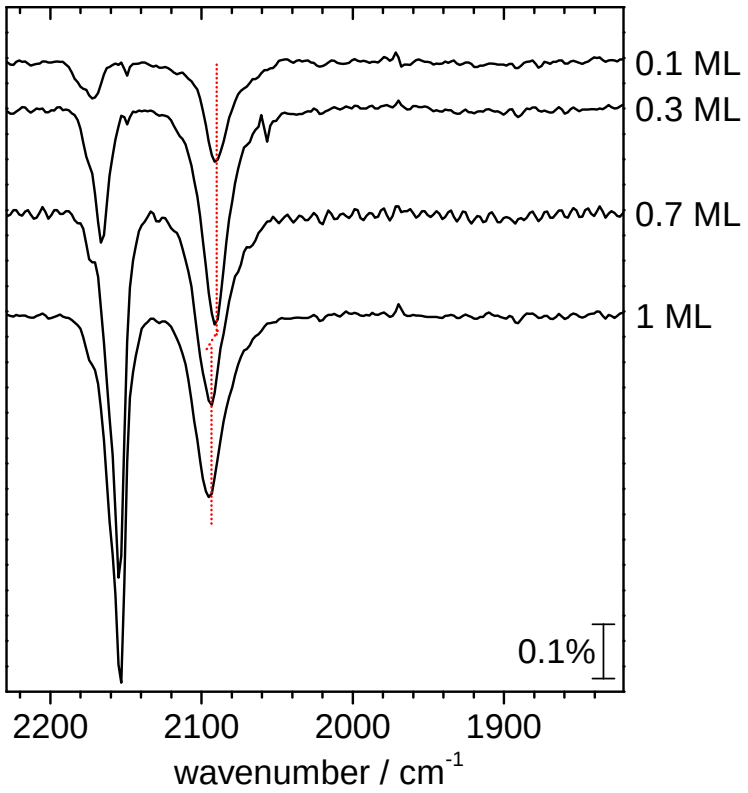

Figure 4.13: IR spectra of 1 Å Cu grown at 35 K on annealed MgO(100) film and annealed to 650 K prior CO adsorbtion

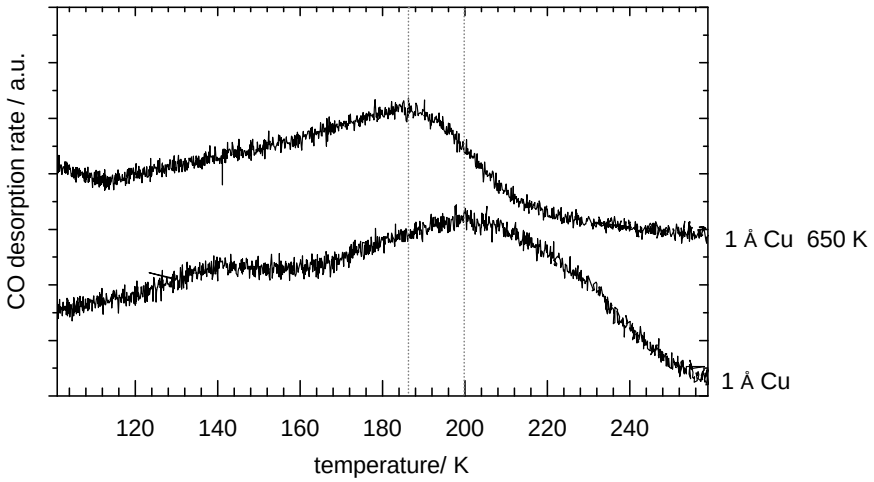

Figure 4.14: TPD spectra of 1 Å Cu on annealed MgO(100) film

Qualitatively the IR and TPD spectra of 1 Å Cu show a similar behavior as for the 2 Å Cu case discussed above except the new IR feature at around 2018 cm^{-1}. This feature is rather unexpected, because it does not fit into CO stretching frequencies observed on Cu single crystal surfaces. In an attempt to unravel its nature, isotope mixing experiments (^{12}CO:^{13}CO = 1:1) were performed on the low temperature deposits (1 ÅCu, T_{dep} = 35 K, annealed MgO(001) film; Fig. 4.15). With increasing CO coverage, the spectra reveals a doublet structure expected for CO on MgO (2160 and 2090 cm^{-1}) and a broad feature whose center shifts from about 2060 cm^{-1} at low coverage to 2080 cm^{-1} at saturation coverage. After exposure of 0.12 ML CO the band at 2066 cm^{-1} is almost symmetric, at 0.2 ML exposure the maximum is shifted to 2083 cm^{-1} with pronounced shoulder around 2030 cm^{-1}, and further increasing the coverage reduces the intensity of the low frequency shoulder progressively. However, no signal assignable to the previously observed peak around 2015 cm^{-1} is observed in the whole coverage range. After annealing the system to 130 K the main peak shifts to the blue (2090 cm^{-1}) and the shoulder becomes a pronounced feature at 2040 cm^{-1}. Annealing to 225 K results in a two peak structure with almost equal intensities at 2085 cm^{-1} and 2035 cm^{-1} which desorb above 250 K as expected based on TPD. The spectra indicate a strong interaction of CO molecules on the particles. In this case the intensities of the infrared bands for ^{12}CO and ^{13}CO are not representative of the relative concentration of these molecules on Cu species. The observed effect is the dramatic intensity transfer from low frequency to high frequency mode due to a dipolar coupling and has been observed on a variety of surfaces [51], [52]. Only after annealing to 225 K when the amount of adsorbed CO molecules becomes small and the interactions weakened, we were able to detect a doublet structure peak (2085 cm^{-1} and 2035 cm^{-1}) representative of individual CO molecules bound to copper particles. The observed behavior is rather typical for particle system exhibiting different adsorption sited with similar IR stretching frequencies and slightly different binding energies. The absence of the rather small peak D around 2015 cm^{-1} can be attributed to an overlap with the broad peak around 2035 cm^{-1}. However, this does not hold for the ^{13}CO peak expected at about 1970 cm^{-1}. In case of a simple splitting into two peaks as observed for the MgO sites the amplitude of the signal should be sufficient to be observed. One possibility would be a more complex distribution of the oscillator strength which makes a detection of the signals impossible, but this cannot be answered based on these experiments.

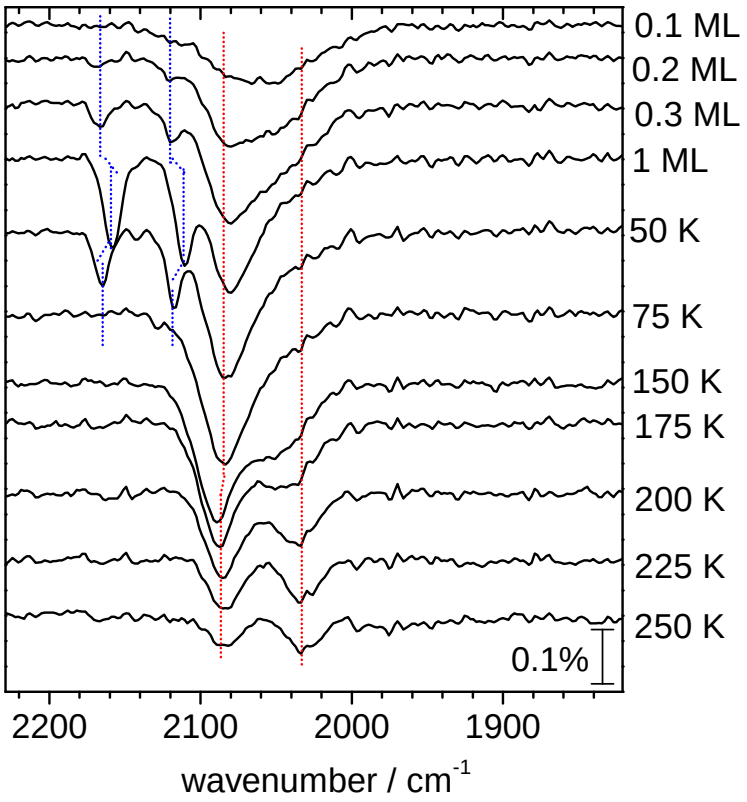

Figure 4.15: IR spectra of 1 Å Cu grown at 35 K on annealed MgO(100) film: mixed isotopes experiment

What happens if the Cu particles become even smaller and the likelihood to prepare individual Cu atoms increases? To answer this question a smaller amount of 0.15 Å Cu was deposited at 35 K on an annealed MgO(001) film. The infrared spectra for different CO coverage are reported in the topmost spectra of Fig. 4.16. The features marked in blue can be assigned to spurious signals originating from the IR spectrometer. The IR spectra exhibits the well known signals of CO on the MgO film on the high energy side as well as two peaks around 2018 cm^{-1} (D) and 1880 cm^{-1} (C). The small peak C is visible only at CO coverage lower than 0.1 ML CO. In low CO coverage regime, the position of peak D is at 2018 cm^{-1} and it shifts to 2012 cm^{-1} for a CO exposure of 0.3 ML. For higher exposures the signal is hardly visible (0.7 ML) or completely absent (saturation coverage). Thus, no features attributed to CO bound to deposited Cu can be detected. TPD spectra show no distinct Cu related CO desorption either which might be due to the small amount of deposited copper and a rather broad desorption peak. This is not to say that the surface is free of Cu. The presence of Cu on the surface can be verified by annealing experiments. As shown in the lower traces of Fig. 4.16 annealing above 60 K leads to the formation of an IR signal around 2100 cm^{-1} which can be assigned to CO bound to Cu particles. It is interesting to note that this signal grows in intensity even though no other CO signals are present which implies that Cu is not only present on the surface, but it also carries the necessary CO to form CO covered Cu particles observed in the IR spectra. Based on this annealing experiment it is expected that growth of 0.15 Å Cu at 300 K on the annealed MgO(001) film will lead to the formation of Cu particles as characterized by an IR signal of adsorbed CO molecules around 2100 cm^{-1}. The experiment for this preparation reveals exactly this behavior. A single broad line centered around 2090 cm^{-1} is observed for the whole coverage regime (see Fig. 4.17). Thus we can conclude that room temperature deposition yields only Cu particles, in agreement with previous studies [64], [84], [81], [82].

What is the nature of the species which give rise to the strongly red-shifted IR bands C and D? With respect to peak C it is important to remember that a peak in this range was observed for Cu(111) and assigned to bridge bonded CO [69], [70], [92]. However, on the single crystal surface these species are present only at high coverage while peak C is a low coverage species. In addition it is only observed for low amounts of Cu which renders the correlation with a high coordinated species unlikely. Due to the rather low

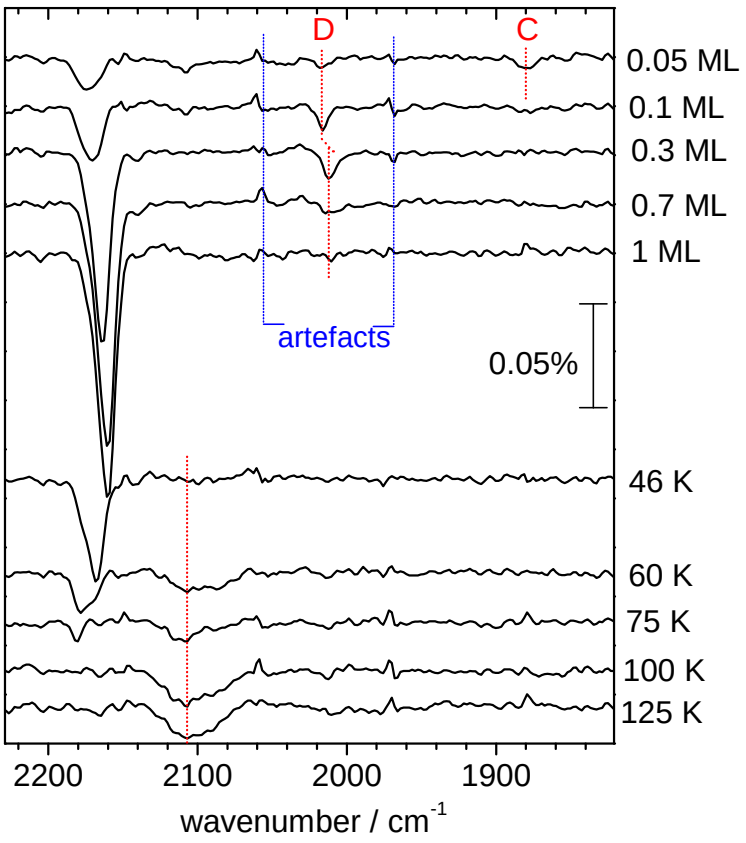

Figure 4.16: IR spectra of 0.15 Å Cu grown at 35 K on annealed MgO(100) film

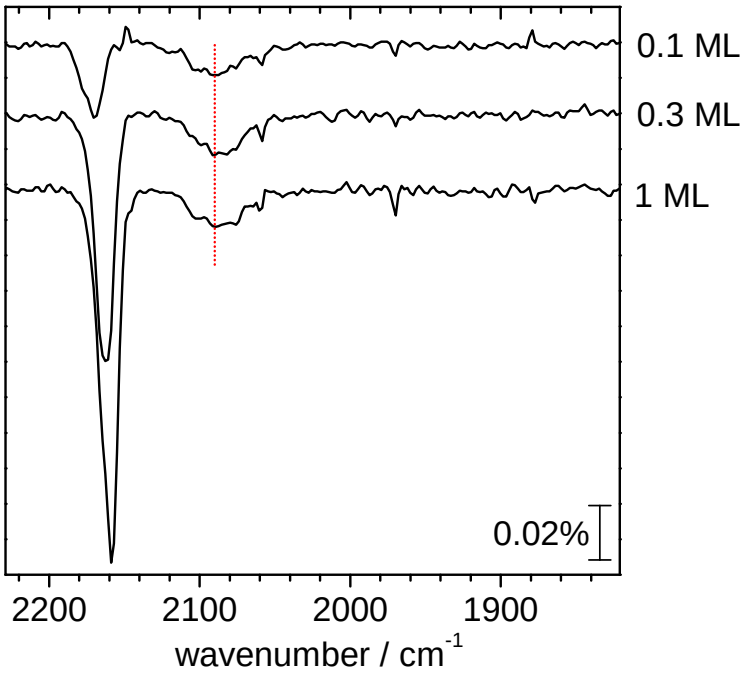

Figure 4.17: IR spectra of 0.15 Å Cu grown at 300 K on annealed MgO(100) film

Cu coverage and low deposition temperature it is tempting to assign these features to CO bound to individual Cu atoms. This would imply that the IR peaks have to behave as expected for metal carbonyls. In an attempt to substantiate this assignment of the peaks around 1880 cm^{-1} and 2018 cm^{-1} spectroscopically, a CO isotope mixing (^{12}CO:^{13}CO = 1:1) experiment was performed (Fig. 4.18). The peak related to CO bound to MgO(001) becomes a doublet structure (2160 and 2090 cm^{-1}) with an intensity ratio of 1:1. The signal at 2015 cm^{-1} splits into a triplet (2016 cm^{-1}, 1997 cm^{-1}, 1969 cm^{-1}) with an intensity ratio of approximately 1:2:1. Based on the isotope pattern it is readily concluded that two CO molecules have to be strongly coupled within this species. Thus, the peak is assigned to a Cu di-carbonyl species. In case of a di-carbonyl it is expected that each molecule has two modes a symmetric and an asymmetric stretching mode. In the spectra only one of these modes is observed. The absence of the second line is due to the IR surface selection rule which restricts observable modes to those with a dynamic dipole moment perpendicular to the surface. Thus, it is expected that only the symmetric stretching mode of the di-carbonyl can be detected. The assignment of the doublet structure at 1881 cm^{-1} and 1831 cm^{-1} with an intensity ratio of 1:1 is less straight forward. The spectra show that there is only one CO molecule associated with this peak. Together with the knowledge acquired on single crystal surfaces the signal is tentatively assigned to a Cu mono carbonyl species. All attempts to prove a transformation of the mono-carbonyl species (1881 cm^{-1}) into a di-carbonyl (2016 cm^{-1}) were unsuccessful.

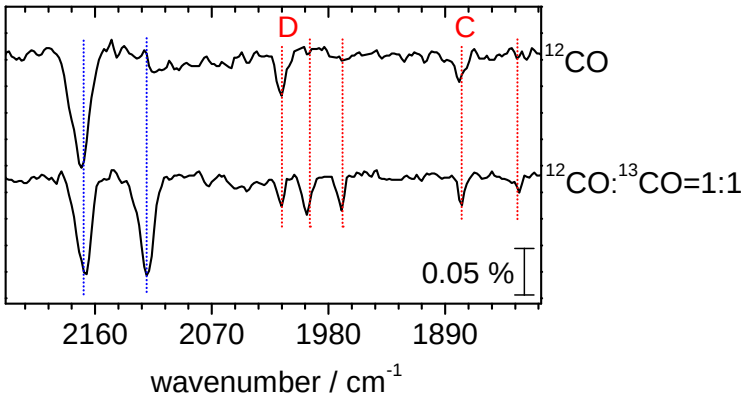

Figure 4.18: IR spectra of 0.15 Å Cu grown at 35 K on annealed MgO(100) film: ^{12}CO and mixed isotopes experiment at 0.15 ML CO coverage

To gain insight into the thermal stability of the Cu species C and D, annealing experiments were performed starting at a CO coverage of 0.15 ML (Fig. 4.19). The small

peak C broadens with increasing CO coverage from 0.02 to 0.1 ML and vanishes irreversibly after annealing to 50 K (third trace Fig. 4.19), which was proven independently by subsequent CO adsorption (data not shown). Concomitantly peak D shifts back to higher frequency as observed at low CO coverage and the signal gains intensity. Annealing to higher temperatures reduces the intensity which finally disappears after annealing to 125 K. This is an irreversible process as shown by subsequent re-adsorption of CO (data not shown). From these experiments it is readily concluded that the di-carbonyl species D is more stable than the mono-carbonyl, but both are stable only at low-temperatures. However, at present it is not clear if this reduced stability of the mono-carbonyl is due to an enhanced surface mobility or a reduced binding energy of the CO molecules. It is worth noting, that annealing to temperatures higher than 60 K leads to the formation of a broad band around 2110 cm^{-1} which can be assigned to CO bound to Cu particles. During annealing the signal of CO on Cu particles around 2110 cm^{-1} grows at the expense of peak D. Thus, it is concluded that the particles are formed out of the carbonyl species. It particularly interesting that these experiments provide direct evidence for the mobility of the di-carbonyl species, because of the formation of CO covered Cu particles in the absence of other CO molecules on the surface. This would also provide an explanation for the observation in the annealing experiment starting at saturation coverage (see Fig. 4.16). The main difference between the two scenarios is that the di-carbonyl species become invisible for high CO coverage on the MgO surface. While dipole interaction allow to explain the absence at high CO coverage the lack of a signal after annealing to 75 K where the terrace as well as a large fraction of the defect bound CO is already desorbed points to an alteration of the di-carbonyl by the presence of the surrounding CO molecules.

To the best of our knowledge, no such species have been reported for well defined copper systems in the literature. In an Ar matrix isolation study Huber *et al.* [66] have shown the existence of mono and di- carbonyls with CO stretching frequency 2010 cm^{-1} and 1890 cm^{-1}, respectively. More recently Zhou et al. have confirmed the assignment of the adsorptions at 2029 cm^{-1} and 1890 cm^{-1} to mono- and di-carbonyls, respectively, based on isotopic substitution as well as density functional calculations [67]. The frequencies are very similar to the ones observed on the surface, however, the assignment to mono and di-carbonyl species is reversed. One has to bear in mind that the bonding of the

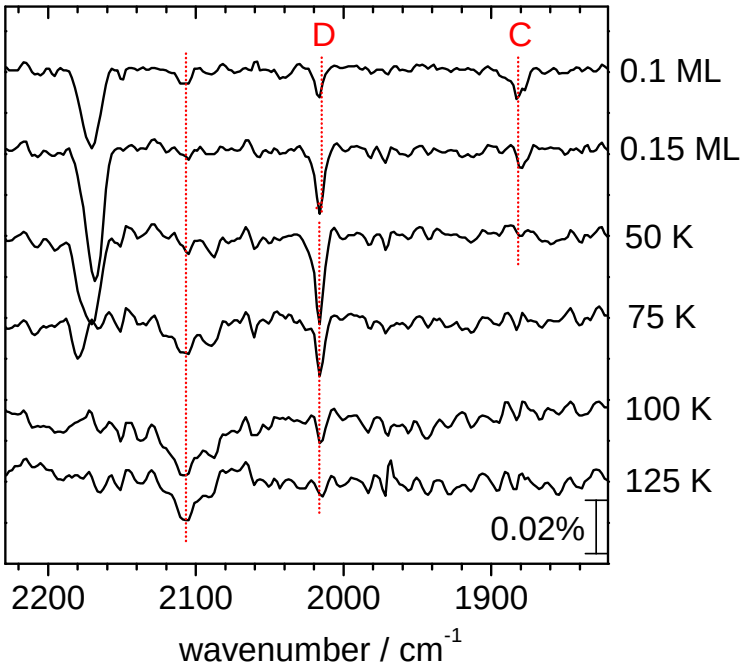

Figure 4.19: IR spectra of 0.15 Å Cu grown at 35 K on annealed MgO(100) film below 0.15 ML CO coverage

copper carbonyls to the oxide can change the properties of the species as compared to the rare gas matrix considerably. To this end it was found that copper di-carbonyl is a linear molecule, both experimentally [66] and theoretically [68], while this is not compatible with the experimental results, because of the surface selection rule.

There are some investigations on powder catalysts reporting CO stretching frequencies in this range. Dandekar and Vannice [72] for example have found a broad band at 2003 cm^{-1} after low temperature adsorption of CO on a reduced Cu/Al_2O_3 catalyst which they have tentatively assigned to bridged species. On a reduced Cu/SiO_2 catalyst Knözinger and coworkers [73] have found two bands at 2045 and 2018 cm^{-1}. The peak at 2045 cm^{-1} was assigned to $Cu^0(CO)_2$ complexes. While the other signal (2018 cm^{-1}) was assigned to linear mono-carbonyls, because of the fact that the latter is formed out of the former species after reduction of the CO pressure. This renders the mono-carbonyl more stable than the di-carbonyl which is in contrast to the present experiments. However, it has to be kept in mind that a direct correlation of the present results with those obtained on powdered material can be hampered by the complexity of these materials as well as the difference in experimental conditions.

In an attempt to unravel the influence of low-coordinated sites of the MgO surfaces on

the nucleation of Cu species, a nominally identical amount of 0.15 Å Cu was deposited at 35 K on a rough MgO(001) film. This system was exposed to a small amount of CO to allow for an observation of peaks C and D. The corresponding IR spectra are shown in Fig. 4.20 as colored traces. For comparison the IR spectra taken on the annealed film are superimposed as black traces. There are several points worth to mention:

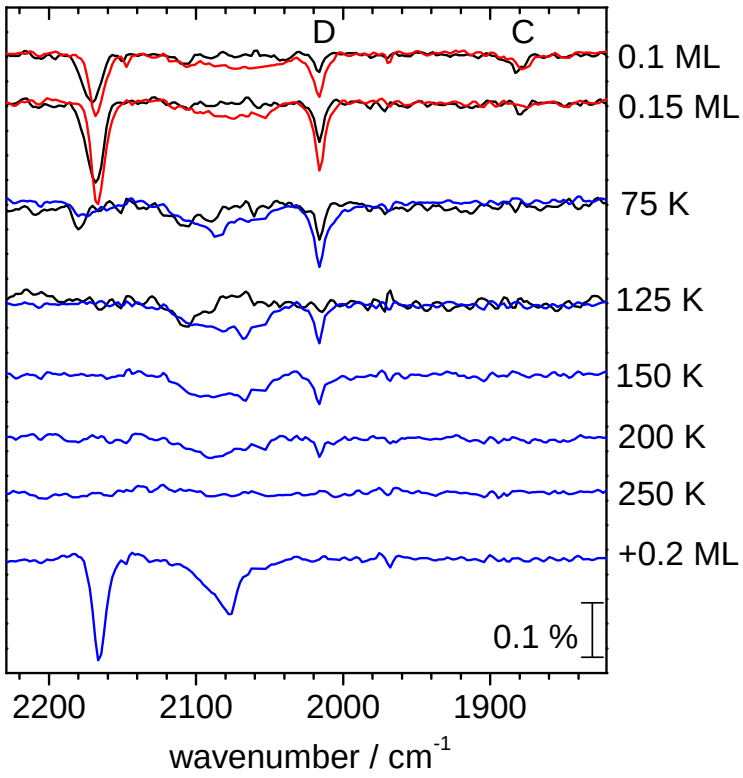

Figure 4.20: IR spectra of 0.15 Å Cu grown at 35 K on annealed (black lines) and rough (color lines) MgO(100) film

The broad band around 2080 cm^{-1}, assigned to Cu particles, can be observed on rough MgO films above a CO exposure of 0.1 ML, while such a signal was absent on the annealed surface. This points to the fact that nucleation on steps, corners and kinks of MgO stimulate the formation of Cu particles. In addition, the intensity of peak D is also enhanced as compared to the annealed film which suggests that these species are also nucleated on morphological defects. The simultaneous increase of both the signal of CO on particles and of Cu di-carbonyl species for the same nominal amount of Cu requires that the particle size has to decrease considerably so that the total number of surface atoms increases. However, slight variations ($\pm$ 20%) of the total amount of Cu between different preparations is also possible. On the other hand the behavior and intensity of

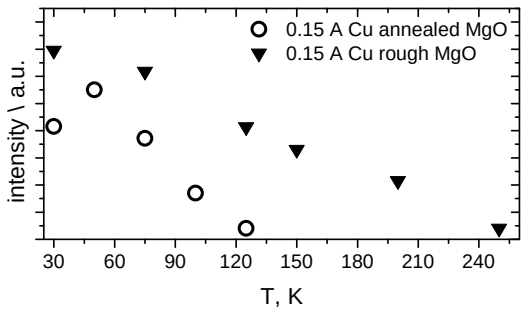

Figure 4.21: 0.15 Å Cu on rough and annealed MgO(100) film: comparison of peak intensities at 2015 cm^{-1}. Starting point at 30 K is at 0.15 ML CO coverage

the small peak C is not changed with increased amount of low-coordinated MgO sites (Fig. 4.20). Isotope mixing experiments (^{12}CO:^{13}CO=1:1) on the rough film (data not shown) show the same splitting pattern which confirms the previous assignment as mono-carbonyl (1880 cm^{-1}) and di-carbonyl (2015 cm^{-1}), respectively. It is interesting to note that the intensity of peak D is not only systematically higher for the rough film (Fig. 4.21) but it also disappears irreversibly at higher temperature (250 K) and with a slower rate. The enhanced stability might be due to a change in the relative population of di-carbonyls at different morphological sites (edges, corners, kinks etc.) whose relative concentration is different for an annealed or a rough film. The presence of CO bound at such a high temperature corroborates further the previous conclusion that it is the carbonyl which is mobile on the surface.

The whole set of experiments on this small amount of Cu (0.15 Å) allows to draw the following conclusions: based on the coverage and temperature behavior and isotope mixing experiments it is possible to assign the IR signals C and D to mononuclear Cu carbonyls with one and two CO molecules per metal center, respectively. The di-carbonyls becomes mobile at higher temperature which leads to the aggregation into copper particles.

4.2.2 Cu on MgO(100) films containing color centers

Defect sites are assumed to be more reactive and the properties of metal atoms or particles adsorbed on such sites may be qualitatively different from those nucleated on regular surface sites. Particularly, color centers are considered important in this respect, because of their electron donating character which is thought to result in charged metal metal particles [75]. This aspect gain considerable interest after a combined experimental

and theoretical study came to the conclusion that color centers are able to change the catalytic properties of deposited Au particles due to this effect [40].

Despite this general perception a direct experimental was given only recently. In a combined STM, EPR and IR study Sterrer et al. showed that Au clusters bound to color centers on MgO(100) films become indeed negatively charged [76]. However, this result prompted the question whether charge transfer is a more general phenomenon also for other metal, or if it is a special property of Au with its rather large electron affinity which is thus particularly prone to the observed electron transfer. To elucidate this question a combination of electron paramagnetic resonance and infrared spectroscopy is employed to characterize the interaction of Cu with color centers on the MgO surface.

The upper trace in Fig. 4.22 shows the EPR spectrum around the free electron g-value measured after bombarding a rough MgO(001) film with electrons. The spectrum reveals a signal around g = 2.000 which can be assigned to paramagnetic F_s^+-centers. As shown previously these centers are located at edge sites (and to a smaller extend on the corners) of the MgO islands [48]. After deposition of 0.15 Å Cu at 40 K onto this surface, the EPR signal of the color center is partially quenched. This is in contrast to the situation found for Au deposition. For Au Sterrer *et al.* [76] showed that deposition of 0.015 Å Au at 30 K on a comparable substrate results in complete depletion of EPR signal from F_s^+ centers on the MgO-film which was used to prove the nucleation of Au at these sites. Therefore the partial quenching of the color center signal after depositing a ten times larger amount of Cu atoms indicates, that Cu interacts much weaker with F_s^+ centers than Au.

Fig. 4.23 shows the corresponding CO-IR spectra as a function of CO coverage (red traces) and annealing temperature (blue traces). For comparative reasons the signal of the electron bombarded MgO surface is overlayed as black traces. As seen from the red traces the MgO surface with Cu deposits exhibits four IR signals in addition to the well known one around 2160 cm^{-1} arising from CO on the MgO surface. At low CO coverage a broad band around 2070 cm^{-1}, and peaks at 2016 cm^{-1}, 1881 cm^{-1}, and 1740 cm^{-1} are observed. With increasing coverage the broad feature shifts to the blue (2075 cm^{-1}), the peak at 1881 cm^{-1} is depleted, and the two other peaks are red shifted to 2006 cm^{-1}, and 1720 cm^{-1}, respectively. The broad signal around 2070 cm^{-1} is readily assigned to CO bound to Cu particles. The peak at 2016 cm^{-1} is also known from the previous experiments and was assigned to a Cu di-carbonyl. The fact that we are able to detect

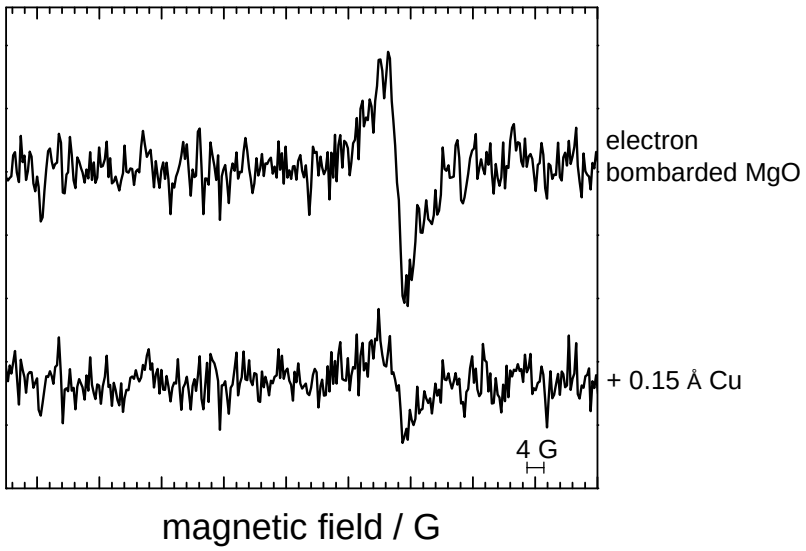

Figure 4.22: EPR spectrum of electron bombarded MgO(100) film and EPR spectrum after deposition of 0.15 Å Cu at 30 K on electron bombarded MgO(100) film

peak D at saturation CO coverage is consistent with the assumption of the increase of the amount of these copper species with increase of steps and edges of MgO surface.

Signals at 1881 cm^{-1} (A) and 1740 cm^{-1} (B) have been observed for electron bombarded MgO surface and were assigned to CO adsorbed on F_s^+- and F_s^0-centers as discussed in detail above. Please note that a band around 1880 cm^{-1} was also found for the deposition of Cu onto MgO surfaces and was designated as peak C in the previous section. Based on the coverage dependence and the width signal this peak can be assigned to the mono-carbonyl (Peak C). The behavior of peak B at 1740 cm^{-1} is consistent with that found for the electron bombarded MgO, however, the signal is broadened and its intensity partially reduced high coverage which might indicate some modification of environment of this site.

Based on this results it can be concluded that there no evidence for a new IR band which cannot be assigned based on the previous experiments. However, the results show that the IR signal corresponding to CO adsorbed on the F-centers is quenched (Peak A) or attenuated (Peak B) upon Cu deposition. This confirms the nucleation of Cu on the F-centers -in particular on the sites giving rise to peak (A)- however, there no indication for charge transfer from the F-centers onto the Cu as found for the case of Au deposits.

During the annealing of the system, the spectrum undergoes the following changes. The broad band at 2075 cm^{-1} assigned to Cu particles gains intensity up to annealing to 125 K and transforms into a peak at 2090 cm^{-1} with a shoulder at the low frequency side. Upon

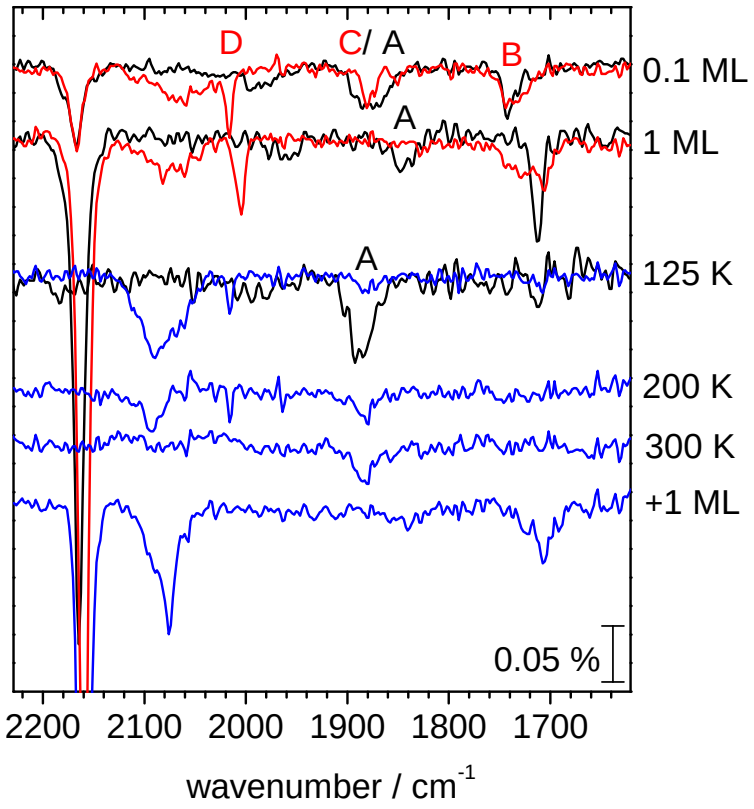

Figure 4.23: IR spectra of 0.15 Å Cu grown at 35 K on electron bombarded MgO(100) film (color lines) and electron bombarded MgO(100) film (black lines)

further annealing the signal intensity decreases and vanishes above 250 K. Peak D shifts back to 2016 cm^{-1} upon annealing to 125 K and its intensity is concomitantly reduced to about a third of the original value. Upon further annealing to higher temperatures the signal disappears at 250 K. This is in the line with the results obtained for copper on rough MgO without color centers. The peak at 1720 cm^{-1} from MgO color centers disappears after heating the system to 60 K, which is consistent with results obtained on an electron bombarded MgO films without copper deposition. An interesting modification of the spectrum occurs after annealing at 125 K. The signal around 1880 cm^{-1} reappears and with increasing temperature up to 300 K it grows in intensity and shifts to 1886 cm^{-1}. Based on the temperature behavior these feature can be assigned to CO bound on the F-center characterized by peak A. This indicates a redistribution of Cu away from the F-center. Readsorption of CO at 35 K results in sharp peak at 2075 cm^{-1} with a shoulder at 2090 cm^{-1} assigned to CO bound to Cu particles, and peaks at 1840 and 1710 cm^{-1} which can be assigned to CO bound on color centers.

The previous experiment indicates that in case of Cu F-centers are not the most stable adsorption sites. Thus, it is expected that growth of Cu at elevated temperatures will reduce the interaction of Cu with color centers even further. To prove this expectation 0.15 Å Cu was deposited at 300 K on an electron bombarded MgO(100) film. The EPR signal of the F_s^+ centers taken prior and after the Cu deposition is shown in Fig. 4.24. The EPR signal is only weakly attenuated after the Cu deposition which indicates that indeed Cu does not nucleate as effectively on the paramagnetic F-center as at low temperature.

The IR spectra of the corresponding preparation are shown as red traces in Fig. 4.25. At low coverage three Cu related peaks at 2060 cm^{-1} (Cu particles), 1880 cm^{-1} (Peak A), and 1740 cm^{-1} (Peak B) are observed. The Cu particle signal shifts to the blue (2080 cm^{-1}) with increasing coverage while the other two shift to the red exactly as found for the electron bombarded MgO surface (black traces). First it is worth noting that peak A is observed under these conditions which was not detected for Cu deposited at low temperature. While the behavior of peak A is qualitatively different for the 300 K deposits the behavior of peak B is -if at all- only slightly modified. Peak B is found to be broadened and reduced in intensity for saturation coverage as it was observed for the low temperature deposits. The IR signals indicative of Cu mono and di-carbonyls were not detected for the 300 K deposits in line with the observations made for pristine MgO

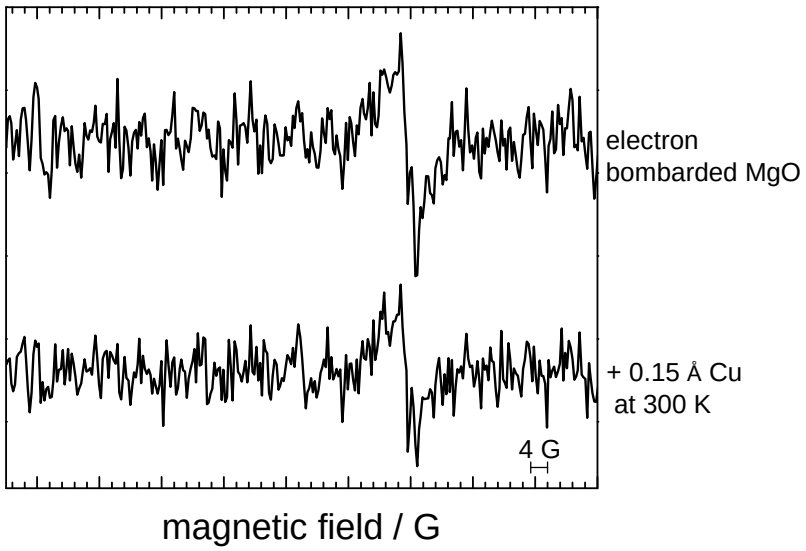

Figure 4.24: EPR spectra of electron bombarded MgO(100) film and EPR spectrum after deposition of 0.15 Å Cu at 300 K on electron bombarded MgO(100) film

films. The temperature behavior was probed by annealing the system to 125 K. This results in a blue shift and an intensity increase of the Cu-particle signal. In addition peak B disappears in line with the expectation based on the previous experiments and peak A shifts back to higher frequency even though the gain in intensity is less pronounced than it is found for the electron bombarded surface (black trace).

Based on these experiments, the following conclusions can be drawn:

i) Deposition of small amounts of Cu onto MgO films exhibiting color centers leads to a nucleation of Cu both on F_s^+ and F_s^0 sites. This is in agreement with theoretical calculations [78], [79], [80]. These investigations predict that Cu binds preferentially to the oxygen anions of MgO(100), especially, to low-coordinated oxygen sites, or, if present, to oxygen vacancies. However, there seem to be differences between the two F-centers. The EPR results show that the interaction with the paramagnetic color center is rather weak which is in contrast to Au [76]. This is in line with the IR results. For Cu deposition at low temperature peak A, which was tentatively assigned to the F_s^+ centers, is largely quenched but becomes partly available after annealing to 125 K. For deposition at 300 K these sites are only weakly perturbed by the Cu deposits. On the other hand the influence of Cu deposits on peak B, which was assigned to F_s^0 centers, is almost independent of the deposition temperature. This is consistent with theoretical calculations [78], which predict stronger binding of Cu atoms on F_s^+ centers than on F_s^0 centers.

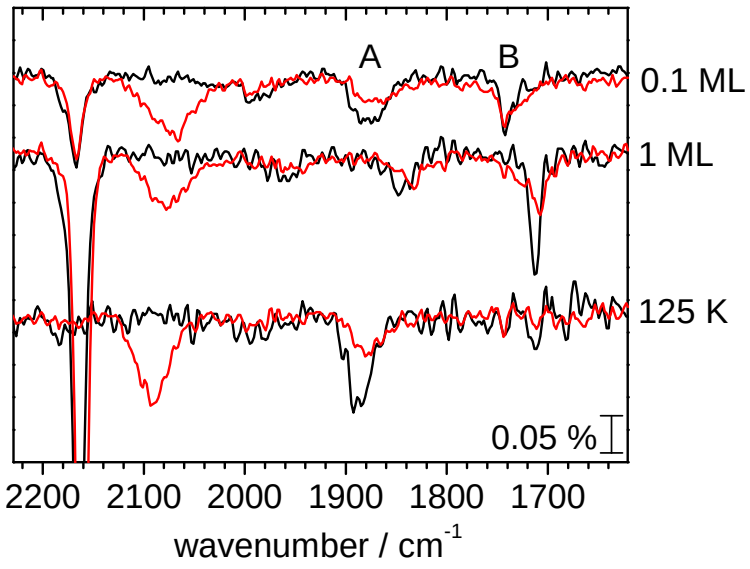

Figure 4.25: IR spectra of 0.15 Å Cu deposited at 300 K on electron bombarded MgO(100) film (red lines) and electron bombarded MgO(100) film (black lines)

ii) Cu-Cu interaction dominates the Cu-MgO interaction. While atomic like species can at room temperature even with the presence of oxygen vacancies.

iii) In case of Au particles nucleated on color centers a characteristic red shift of the IR signal is observed which is due to an enhanced π-back donation and indicative for a charging of the Au particles [76]. In contrast, the Cu deposits investigated here show no additional signal shifted to lower frequencies. Thus, it is not possible to provide evidence for a charge transfer from the color center to the Cu particles. This is not sufficient to conclude that such charge transfer does not occur. A possible reason for this failure might be a very weak binding of CO on negatively charged Cu atoms or particles which hampers the observation.

The different behavior of Cu and Au may be rationalized in terms of the electron affinities [95][3]. According to the classical molecular orbital interpretation of the charge redistribution in a molecular metal-donor (M-D) systems the electron transfer to the metal (M) will depend on the ionization potential (IP) of the donor (D) and the electron affinity (EA) of the metal. For the given of color centers on an oxide surface it is more appropriate to compare the position of the highest occupies orbital of the color center with respect to the vacuum level to the EA of gold or copper. The values of EA for Cu and Au are

[3]The electron affinity is the energy released when an electron is added to a neutral atom, a positive electron affinity indicates that energy is released on going from atom to anion.

very different, namely, 1.236 and 2.229 eV, respectively [94]. This already indicates that the highest occupied molecular orbital of Cu is substantially higher in energy than that of Au which renders a charge transfer based on these very simple consideration unlikely. This simple picture neglects all changes of the of the position of the participating orbital basically assuming very weak interaction. A more thorough discussion of the effects of Cu binding to MgO surface sites requires the theoretical calculations.

Chapter 5

Conclusions

In the first part of this work we have discussed the interaction of the CO molecule with MgO(100) single crystalline thin films, exhibiting F_s^+ and F_s centers. Two new IR bands associated with CO bound on color centers have been observed around 1850 cm^{-1} and 1710 cm^{-1}. The strong red shift of the CO stretching frequency was explained by electron donation from the F-center onto the CO molecule. This implies the formation of CO^- radicals. Based on comparison with theoretical calculations the IR band at 1850 cm^{-1} was assigned to CO on F_s^+-centers giving rise to a CO^-/F_s^{2+} charge transfer complex, and the band at 1710 cm^{-1} to the formation of a CO^-/F_s^+ complex formed by adsorption of CO on an F_s^0 centers. However, this assignment is tentative at the moment and needs further theoretical support. The required theoretical calculations are currently done in the group of Joachim Sauer at the Humboldt University, Berlin.

In the second part of this thesis Cu atoms and clusters deposited on MgO(100) films were studied as a function of copper coverage, depositing and annealing temperature with a particular focus on the influence of morphological defects as well as color centers of MgO films on the properties Cu species.

TPD and IR spectroscopy results have shown, that the deposition of 2 Å Cu on well ordered MgO(100) film results in formation of copper particles. Low-temperature deposition yields Cu particles with a high concentration of step/edge defect sites, while annealing to 650 K or room temperature deposition results in particles exhibiting larger low index facets as expected based on thermodynamic considerations.

IR studies have shown, that low temperature deposition of small amount (0.15 Å) of copper on well ordered MgO(100) film results in formation of Cu species different from

particles. It was possible to assign these IR signals new mono-carbonyl and a di-carbonyl species with CO IR stretching frequency around 1880 and 2015 cm^{-1}, respectively. These copper carbonyls were found to aggregate into copper particles with annealing. It was shown, that the increase of the amount of morphological defects of MgO surface stimulates formation of Cu particles and increases the amount of di-carbonyl Cu species.

Using a combination of IR and EPR spectroscopy, it was shown that deposition of small amount (0.15 Å) of Cu at low temperature onto surfaces exhibiting color centers leads to a nucleation of Cu onto paramagnetic and diamagnetic color centers. Cu-Cu interactions were found to dominate over Cu-MgO surface interactions at room temperature even with the presence of color centers. However, differences were found for F_s^+ and F_s^0 centers. While the interaction with the F_s^0 seems to be weak the interaction with certain F_s^+ centers is considerably stronger. No indication for IR signal shift to lower frequencies due to a charging of the Cu particles was detected, which could be explained by the relatively small electron affinity of copper. Although, further theoretical support is required.

Bibliography

[1] H. Wennerstroem, S. Lidin, *Scientific Background on the Nobel Prize in Chemistry 2007* (The Royal Swedish Academy of Sciences, Stockholm, Sweden 2007)

[2] R. Schlögl, Angew. Chem. Int. Ed. Engl. **32** (1993), 1524

[3] H. Bluhm et al., MRS Bulletin **32** (2007), pp. 1022-1030

[4] D. W. Goodman, J. Cat. **216** (2003), pp. 213–222

[5] D.W. Goodman, R.D. Kelley, T.E. Madey, J.T. Yates, J. Catal. **63** (1980), 226

[6] P.L.J. Gunter, J.W. Niemantsverdriet, F.H. Ribeiro, G.A. Somorjai, Catal. Rev. Sci. Eng. **39** (1997), 77

[7] C.T. Campbell, Surf. Sci. Rep. **27** (1997), 1

[8] C.R. Henry, Surf. Sci. Rep. **31** (1998), pp. 235-325

[9] H.-J. Freund, M. Baumer, J. Libuda, T. Risse, G. Rupprechter, S. Shaikhutdinov, J. Catal. **216** (2003), pp. 223-235

[10] M. Chen, D.W. Goodman, Acc. Chem. Res. **39** (2006), pp. 739-746

[11] H. J. Freund, Phys. Status Solidi B **192** (1995), 407

[12] E. Giamello, D. Murphy, M. C. Paganini, Colloids and Surfaces A **115** (1996), pp. 157-170

[13] J. Libuda, T. Schalow, B. Brandt, M. Laurin, S. Schauermann, Microchim. Acta **156** (2007), pp. 9-20

[14] H. J. Freund, J. Libuda, M. Baumer, T. Risse, A. Carlsson, Chem. Record, **3** (2003), pp. 181–200

[15] M. C. Wu, C. M. Truong, K. Coulter, D. W. Goodman, J. Am. Chem. Soc. **114** (1992), 7565

[16] M. C. Gallagher, M. S. Fyfield, L. A. Bumm, J. P. Cowin, S. A. Joyce, Thin Solid Films **445** (2003), 90

[17] S. Schintke, S. Messerli, M. Pivetta, F. Patthey, L. Libioulle, M. Stengel, A. D. Vita, W.-D. Schneider, Phys. Rev. Lett. **87** (2001), 276801

[18] Z. Dohnalek, G. A. Kimmel, S. A. Joyce, P. Ayotte, R. S. Smith, B. D. Kay, J. Phys. Chem. B **105** (2001), 3747

[19] S. Benedetti, H. M. Benia, N. Nilius, S. Valeri, H. J. Freund, Chem. Phys. Lett. **430** (2006), pp. 330–335

[20] H.L. Meyerheim et al., Phys. Rev. Lett. **87** (2001), 076102

[21] F. Seitz, Rev. Mod. Phys. **18** (1946), pp. 384-408

[22] M. Klaua et al., Phys. Rev. B **64** (2001), 134411

[23] J. Carrasco, N. Lopez, F. Illas, H.-J. Freund, J. Chem. Phys. **125** (2006), 074711

[24] M.-C. Wu, C. M. Truong, D. W. Goodman, Phys. Rev. B **46** (1992), 12688

[25] M. Kaupp, M. Bohl, V.G. Malkin, *Calculation of NMR and EPR Parameters* (Wiley VCH, Weinheim 2004)

[26] M. Valden, X. Lai, D. W. Goodman, Science **281** (1998), 1647

[27] G. Pacchioni, Solid State Sciences **2** (2000), pp. 161–179

[28] G. Pacchioni, CHEMPHYSCHEM **4** (2003), pp. 1041 - 1047

[29] F. Delannay, *Characterization of heterogeneous catalysts* (Dekker, New York 1984)

[30] C. P. Poole, *Electron spin resonance: a comprehensive treatise on experimental techniques* (Wiley, New York 1983)

[31] J. P. Roth, *Vacuum Technology* (North-Holland,Amsterdam 1982)

[32] R. T. Weber, *EMX user's manual*, Bruker Instruments (1995)

[33] N.G. Yaroslavsky, A.N. Terenin, Dokl. Akad. Nauk SSSR, **66** (1949), 885

[34] L.H. Little, *Infrared Spectra of Adsorbed Species* (Academic, New York 1966)

[35] A.V. Kiselev, V.I. Lygin, *Infrared SPectra of Surface Compounds* (Wiley, New York 1975)

[36] M. C. Wu, ; J. S. Corneille, J. W. He, C. A. Estrada,D. W. Goodman, Chem. Phys. Lett. **182** (1991), 472

[37] Y. Farge; M. P. Fontana, *Electronic and vibrational properties of point defects in ionic crystals* (North-Holland Publ., Amsterdam 1979)

[38] R. F. Wood, H. W. Joy, Phys. Rev. **136** (1946), 451

[39] A. M. Ferrari, G. Pacchioni, J. Phys. Chem. **99** (1995), 17 010

[40] B. Yoon et al., Science **307** (2005), 403

[41] J. Schmidt, T. Risse, H. Hamann, H. J. Freund, J. Chem. Phys. **116** (2002), 10861

[42] M. Sterrer et al., J. Phys. Chem. B **407** (2006), 8665

[43] H. Schlienz et al., Phys. Rev. Lett. **74** (1995), 761

[44] J. Heidberg, M. Kandel, D. Meine, U. Wildt, Surf. Sci. **1467** (1995), pp. 331–333

[45] L. Marchese, S. Coluccia, A. Zecchina, Surf. Sci. **135** (1992), pp. 269–270

[46] G. Pacchioni, Surf. Rev. Lett. **7** (2000), 277

[47] M. Sterrer, T. Risse, H. J. Freund, Surf. Sci. **596** (2005), 222

[48] M. Sterrer et al., Phys. Rev. Lett. **94** (2005), 186101

[49] M. Sterrer, M. Heyde, M. Novicki, N. Nilius, T. Risse, H. P. Rust, G. Pacchioni, and H. -J. Freund, J. Phys. Chem. B **110** (2006), 46

[50] E. Giamello, D. Murphy, L. Marchese, G. Martra, A. Zecchina, J. Chem. Soc. Faraday Trans. **89** (1993), 3715

[51] E. Borguet, H. L. Dai, Chem. Phys. Lett. **194** (1992), 57

[52] P. Hollins, Spectrochim. Acta **43 A** (1987), 1539

[53] B. N. J. Persson, R. Ryberg, Phys. Rev. B **24** (1981), 6954

[54] A. M. Ferrari and G. Pacchioni, J. Chem. Phys. **107** (1997), 2066

[55] L. Marchese, S. Coluccia, G. Martra, E. Giamello, A. Zecchina, Chem. Phys. **29** (1991), 437

[56] P. Hollins, Surf. Sci. Rep. **16** (1992), 51

[57] S.A. Pope, I.H. Hillier, M.F. Guest, E.A. Colbourn, J. Kendrick, Surf. Sci. **139** (1984), 299

[58] G. Pacchioni, G. Cogliandro, P. S. Bagus, Int. J. Quant. Chem. **42** (1992), 1115

[59] L. Chen, R. Wu, N. Kioussis, Q. Zhang, Chem. Phys. Lett. **290** (1998), 255

[60] R. Wu, Q. Zhang, Chem. Phys. Lett. **306** (1999), 205

[61] R. Wichtendahl, M. Rodriguez-Rodrigo, U. Hartel, H. Kuhlenbeck, H.-J. Freund, Phys. Status Sol. App. Res. **173** (1999), 93-100

[62] B.N.J. Persson, R. Ryberg, Phys. Rev. B **24** (1981), pp. 6954 - 6970

[63] J. Pritchard, T. Catterick, R. K. Gupta, Surf. Sci. **53** (1975), pp. 1-20

[64] J. B. Zhou, T. Gustafsson, Surf. Sci. **375** (1997), pp. 221-225

[65] J.-W. He, P. J. Möller, Surf. Sci. **178** (1986), 934

[66] H. Huber, E. P. Kundig, M. Moskovits, G. A. Ozin, J. Am. Chem. Soc. **97** (1975), 2097

[67] M. Zhou, L. Andrews, J. Chem. Phys. **111** (1999), 4548

[68] V. Barone, J. Phys. Chem. **99** (1995), 11695

[69] B. Hayden, K. Kretzschmar, A. Bradshaw, Surf. Sci. **155** (1985), 553

[70] R. Raval, S. Parker, M. Pemble, P. Hollins, J. Pritchard, M. Chesters, Surf. Sci. **203** (1988), 353

[71] F. Mehmood, A. Kara, T. S. Rahman, K. P. Bohnen, Phys. Rev. B **74** (2006), 155439

[72] A. Dandekar, M. A. Vannice, J. Catal. **178** (1998), 621

[73] K. Hadjiivanov, T. Venkov, H. Knozinger, Catal. Lett. **75** (2001), 55

[74] S. Vollmer, G. Witte, C. Woell, Catal. Lett. **77** (2001), 97

[75] M. Valden, X. Lai, D. W. Goodman, Science **281** (1998), 1647

[76] M. Sterrer, M. Yulikov, E. Fischbach, M. Heyde, H. P. Rust, G. Pacchioni, T. Risse, H.-J. Freund, Angew. Chem. Int. Ed. **45** (2006), 2630

[77] S. Abbet, E. Riedo, H. Brune, U. Heiz, A. M. Ferrari, L. Giordano, G. Pacchioni, J. Am. Chem. Soc. **123** (2001), 6172

[78] A. V. Matveev, K. Neyman, I. Yudanov, Surf. Sci. **426** (1999), 123

[79] I. Yudanov, G. Pacchioni, K. Neyman and N. Rösch, J. Phys. Chem. B **101** (1997), 2786

[80] A. Del Vitto et al., J. Chem. Phys. **121** (2004), 7457

[81] V. Musolino, A. Dal Corso, A. Selloni, Phys. Rev. Lett. **83** (1999), 2761

[82] V. Musolino, A. Dal Corso, A. Selloni, Phys. Rev. Lett. **83** (1999), 3242

[83] P. L. Hansen, J. B. Wagner, S. Helveg, J. R. Rostrup-Nielsen, B. S. Clausen, H. Topsoe, Science **295** (2002), 2053

[84] M. Zinke-Allmang, L. C. Feldman, M. H. Grabow, Surf. Sci. Rep. **16** (1992), 377

[85] R. P. Eischens, W. A. Pliskin, S. A. Francis, J. Chem. Phys. **22** (1954), 1786

[86] C. Di Valentin *et al.*, Surf. Sci. **521** (2002), pp. 104–116

[87] G. Pinarello, C. Pisani, A. D'Ercole, M. Chiesa, M.C. Paganini, E. Giamello, O. Diwald, Surf. Sci. **494** (2001), 95

[88] E. Giamello, P. Ugliengo, E. Garrone, J. Chem. Soc. Farad. Trans. **85** (1989), 1373

[89] G. Pacchioni, A.M. Ferrari, E. Giamello, Chem. Phys. Lett. **255** (1996), pp. 58-64

[90] M. Sterrer, T. Berger, O. Diwald, E. Knoezinger, A. Allouche, Topics Cat. **46** (2007), 111

[91] J.C. Cook, E.M. McCash, Surf.Sci. **356** (1996), pp. 445-449

[92] J.C. Cook, E.M. McCash, Chem. Phys. Lett. **313** (1999), pp. 575–581

[93] P.Hollins, K.J. Davies, J. Pritchard, Surf. Sci. **138** (1984), 75

[94] P. Neogrady, V. Kelloe, M. Urban, A.J. Sadlej, Int. J. Quantum Chem. **63** (1997), 557

[95] G. Pacchioni, Surf. Rev. Lett. **7** (2000), 277

[96] B. Cordero, V. Gymez, A.E. Platero-Prats, M. Reves, J. Echeverrha, E. Cremades, F. Barragen, S. Alvarez, Dalton Trans. **21** (2008), pp. 2832-2838

[97] W. Kirstein, B. Krüger, F. Thieme, Surf. Sci. **176** (1986), 505

[98] J. Kessler, F. Thieme, Surf. Sci. **67** (1977), 405

[99] T. Sueyoshi, T. Sasaki, Y. Iwasawa, Appl. Surf. Sci. **562** (1997), 121-122